KfK 3503
April 1983

Neutron Capture and Fission Cross Section of Americium-243 in the Energy Range from 5 to 250 keV

K. Wisshak, F. Käppeler
Institut für Angewandte Kernphysik

Kernforschungszentrum Karlsruhe

KERNFORSCHUNGSZENTRUM KARLSRUHE
Institut für Angewandte Kernphysik

KfK 3503

Neutron Capture and Fission Cross Section of Americium-243 in the Energy Range from 5 to 250 keV

K. Wisshak and F. Käppeler

Kernforschungszentrum Karlsruhe GmbH, Karlsruhe

Kernforschungszentrum Karlsruhe GmbH
ISSN 0303-4003

ABSTRACT

The neutron capture and subthreshold fission cross section of ^{243}Am was measured in the energy range from 5 to 250 keV using ^{197}Au and ^{235}U as the respective standards. Neutrons were produced via the $^{7}Li(p,n)$ and the $T(p,n)$ reaction with the Karlsruhe 3-MV pulsed Van de Graaff accelerator. Capture events were detected by two MoxonRae detectors with graphite and bismuthgraphite converters, respectively. Fission events were registered by a NE-213 liquid scintillator with pulse-shape discriminator equipment. Flight paths as short as 50 - 70 mm were used to obtain optimum signal-to-background ratio. After correction for the different efficiency of the individual converter materials the capture cross section could be determined with a total uncertainty of 3 - 6 %. The respective values for the fission cross section are 8 - 12 %. The results are compared to predictions of recent evaluations, which in some cases are severely discrepant.

ZUSAMMENFASSUNG

Der Neutroneneinfang- und Spaltquerschnitt von Americium-243 im Energiebereich von 5 bis 250 keV.

Der Neutroneneinfangquerschnitt und der Spaltquerschnitt unterhalb der Schwelle von ^{243}Am wurden im Energiebereich von 5 - 250 keV gemessen. Dabei wurden jeweils ^{197}Au und ^{235}U als Standards verwendet. Die Neutronen wurden über die $^{7}Li(p,n)$ und die $T(p,n)$ Reaktion am gepulsten Karlsruher 3 MV Van de Graaff Beschleuniger erzeugt. Zum Nachweis der Einfangereignisse dienten zwei Moxon-Rae Detektoren mit Graphit- und Wismut-Graphit Konvertern. Die Spaltereignisse wurden mit einem NE-213 Szintillator gemessen, der mit einem Impulsformanalysator ausgerüstet war. Flugwege von nur 50 - 70 mm ermöglichten ein optimales Signal zu Untergrund-Verhältnis. Die Daten wurden auf die unterschiedliche Ansprechwahrscheinlichkeit der einzelnen Konvertermaterialien korrigiert. Der Einfangquerschnitt konnte mit einer Genauigkeit von 3 - 6 % bestimmt werden. Im Falle des Spaltquerschnitts beträgt die Genauigkeit 8 - 12 %. Die Ergebnisse werden mit theoretischen Vorhersagen verglichen, die zum Teil stark abweichend sind.

I. INTRODUCTION

During the last years considerable progress has been achieved in measurements of capture and fission cross sections of minor actinide isotopes in the unresolved resonance region[1,2,3,4]. However, ^{243}Am remained as a white spot, for which no experimental data were reported in the literature. Although the half life of ^{243}Am is about a factor of 20 longer than for ^{241}Am its high energetic gamma radiation ($\sim$ 300 keV with 100 % intensity) causes severe problems in capture cross section measurements. The subthreshold fission cross section is low and can be determined only with a very sensitive experimental method and a very clean sample.

Capture in ^{243}Am contributes significantly to the production of ^{244}Cm, which is of importance in fast reactor studies as a strong neutron emitter, and hence affects the total neutron production rate[5]. Several requests for capture cross section measurements have been formulated[5,6,7,8] asking for an accuracy of $\sim$ 10 % in the keV range. The quoted applications are burn-up studies, the build-up of transplutonium elements, neutron shielding of transport casks for spent fuel elements, fuel reprocessing and storage as well as the long term radioactivity hazard.

The very small fission cross section in the subthreshold region is directly of minor importance for reactor applications. However, there is a more general interest for systematic studies of fission barriers and for reliability tests of codes used in data evaluation.

With the present results for ^{243}Am we have completed a series of measurements on minor actinide isotopes[2,3,9,10,11] including $^{240,242}Pu$ and ^{241}Am. The experimental method is to use Moxon-Rae detectors in connection with kinematically collimated neutrons from (p,n) reactions on light nuclei. The samples are positioned at very short flight paths of 5-7 cm to obtain a high neutron flux at the sample position and consequently a favourable signal-to-background ratio.

One of the largest systematic uncertainties of the experimental method is due to the fact that the efficiency of Moxon-Rae detectors deviates slightly from the ideal shape (which increases linearly with gamma-ray energy). To reduce this uncertainty we used in the present experiment two detectors with different converter materials. This allowed for a check of the calculated efficiency correction. Part of the present results have been published in a preliminary form in Refs. 12 and 13.

II. EXPERIMENTAL METHOD

Similar to earlier work by Macklin et al.[14], the principle of the experimental method is to use (p,n) reactions on light nuclei for neutron production at proton energies just above the reaction threshold. In this case the neutrons are kinematically collimated by the center of mass motion of the compound nucleus. All neutrons are emitted within a cone in a forward direction, the opening angle of which is determined by the proton energy. Therefore, further collimation of neutrons is not necessary and flight paths as short as 5 to 10 cm can be used in the experiments. The capture and fission events can be observed by detectors placed at backward angles completely outside the neutron cone.

Details of the experimental technique have been published in Refs. 2, 9 and 10 and therefore only a brief description is given here.

The experimental set-up is shown schematically in Fig.1. The pulsed proton beam of the Karlsruhe 3 MV Van de Graaff accelerator hits a water cooled ^{7}Li or ^{3}H target producing kinematically collimated neutrons in the energy range 5-100 keV and 40-250 keV, respectively.

To optimize the signal to background ratio high beam currents up to 25 μAmp were applied at a repetition rate of 2.5 MHz. This called for an improved target construction as the previously used spraywater cooled tantalum targets were not able to stand such high currents. They were replaced by targets which were developed for activation measurements[15]. The backing consisted of a o.5 mm thick copper layer and cooling is achieved by lateral heat

Two Moxon-Rae detectors with graphite and bismuth graphite converter served for the detection of capture events. As the Moxon-Rae detector cannot distinguish between gamma rays from capture and fission, we had to use a second detector (sensitive to fission events only) for correction. This was a NE-213 liquid scintillator, which was operated with a pulse shape discriminator, to separate fission neutrons from gamma-ray background. From the data recorded with this detector, it was possible to determine the fission cross section of ^{243}Am, too.

All detectors are located at backward angles of 120 deg with respect to the beam axis, completely outside of the neutron cone. They are shielded with lead against the prompt gamma radiation from the neutron target. The intense gamma radiation from the ^{243}Am sample itself was attenuated by lead absorbers of variable thickness in front of the Moxon-Rae detectors.

In addition, two ^{6}Li glass detectors located at flight paths of 50 and 120 cm and under angles of 0 deg and 20 deg to the proton beam axis, respectively, were used as monitors for the neutron flux. While a time-of-flight (TOF) spectrum was recorded from the transmission detector, a pulse height spectrum was measured from the neutron flux monitor at 20 deg. Both spectra and the integrated beam current on the neutron target were used to ensure that all samples were exposed to the same neutron flux.

Four samples were mounted in a low mass sample changer and cycled automatically into the measuring position:

1) ^{243}Am: A pellet of $^{243}AmO_2$ was prepared which after a

sintering procedure was welded into a 0.15 mm thick stainless stell canning.

2) ^{197}Au: A gold sample was used as a standard.

3) graphite: The thickness of this sample was adjusted to give about the same scattering yield as the gold sample.

4) ^{235}U: This sample was used for normalization of the fission correction.

In order to obtain a similar time dependent background, all samples were canned in the same way. Details of the individual samples are compiled in Table I. The flight path was measured daily by means of an eddy current device relative to a gauge made from stainless steel. This allowed for a high reproducibility (< 0.02 mm) of the measured value and increased the absolute accuracy. All manipulations around the target were performed with the ^{243}Am sample in a shielded position of the sample changer.

The capture and fission cross section of ^{243}Am were measured in the low energy range (5 to 100 keV) using the $^{7}Li(p,n)$ reaction and in the high energy range (40 to 250 keV) using the T(p,n) reaction for the neutron production. A variety of individual runs was performed with modified experimental parameters to check for systematic uncertainties.

At low energies, data were taken in four runs at a flight path of $\sim$ 52 mm using different lead absorbers between 0.5 and 2 cm thickness in front of the detectors. Measurements with thick lead absorbers yielded a high signal-to-background ratio and consequently a low systematic uncertainty due to background subtraction. This

uncertainty dominates the total uncertainty at very low energies and the respective data could be evaluated with confidence down to energies of ∿ 5 keV. On the other hand, runs with thin lead absorbes are less affected by gamma absorption in the lead shielding and could therefore be used to check this correction in the high energy range. The different signal-to-background ratios are demonstrated in Fig. 2.

To reduce the systematic uncertainty due to the determination of the flight path two additional runs have been performed at a flight path of 71 mm and with lead shielding of 2. and 1. cm thickness, respectively. In the two measurements with the tritium target a 2 cm thick shielding was used. The respective spectra of these four runs are shown in Figs. 3a and 3b. Details of the individual runs are compiled in Table II.

As an additional check for the influence of the lead shielding in front of the Moxon-Rae detectors the cross section ratio $\sigma_\gamma(^{238}U)/\sigma_\gamma(^{197}Au)$ has been measured for all different lead shieldings and for the unshielded detectors. As the capture gamma-ray spectra of ^{238}U and ^{243}Am are very similar (see Sec. III) these results can be used to estimate the systematic uncertainty caused by the shielding in the ^{243}Am measurement.

The gamma-ray self-absorbtion in the samples was studied by measuring TOF spectra from gold samples with 18 and 40 mm diameter and with thickness between 0.12 and 1 mm. The respective data could be used to estimate the self-absorbtion in ^{243}Am samples, too.

III. DATA ANALYSIS

As the data analysis has been described in detail in Refs. 2,9,10, 11, here the individual steps are summarized only briefly, emphasizing the applied modifications.

III.A. Capture Cross-Section Measurements

1. Transformation to a common flight path:
   Small differences in flight path were observed for sample and reference sample ($\leq$ 0.7 mm) and for the different neutron targets ($\leq$ 0.1 mm). This effect was corrected for in the same way as described in Ref. 2. Thanks to the improved flight path determination and target construction in most of the runs the daily measured flight paths of sample and reference sample differed by less than 0.2 mm. In these cases no correction was applied.

2. Normalization to equal neutron flux: The measuring time for the individual samples of $\sim$ 10 min was determined by integration of the proton beam current to a preselected value. The neutron production rate of the targets decreased slowly with time. Therefore the neutron exposure was largest for the first sample and decreased slightly for all other samples. To correct for this effect we used the spectra measured with the transmission detector and the neutron flux monitor. The resulting normalization factors for any individual cycle turned out to be always less than 1.3 %. Averaged over all runs the difference in neutron flux irradiating sample and reference sample was 0.8 %.

3. Subtraction of time-dependent and time-independent background: This correction was performed in the same way as described for the ^{241}Am measurement in Ref. 2. The related uncertainties are discussed in Section V.

4. Correction for fission events: Due to the low subthreshold fission cross section of ^{243}Am and the high purity of the sample material, this correction is 1.2 % on the average. The first step for the evaluation of this correction is to determine the ratio R of fission neutrons (observed with the fission neutron detector) to fission gamma rays (observed with the Moxon-Rae detector) for the ^{235}U sample. The spectrum of fission gamma rays was obtained from the measured TOF spectrum by subtracting the components due to capture in ^{235}U and capture in the ^{238}U impurity. As the fission correction is very small and the statistical accuracy of the fission neutron spectra is low we renounced on the unfolding procedure described in Refs. 2 and 11 which exactly accounts for the TOF distribution of the fission neutrons. This procedure was approximated by a constant time shift corresponding to the average TOF of the fission neutrons from sample to detector.

   The final fission correction was then calculated from the ratio R defined above and the fission neutron spectrum of the ^{243}Am sample. Differences in $\bar{\nu}$, in the fission neutron energy spectra, and in the total fission gamma energy between ^{243}Am and ^{235}U have been taken into account.

5. Correction for capture in isotopic impurities:
A correction for capture in isotopic impurities was neglected as the sample was enriches to 99.82 % and 0.17 % from the remaining abundance is ^{241}Am, which has about the same capture cross section.

The sample material was chemically purified from plutonium and curium ∿ 3 years before the measurement. In the final analysis no detectable plutonium impurity was recorded. Therefore, the ^{239}Pu content of the sample which might originate from the decay of ^{243}Am, was definitely less than 0.03 %.

6. Correction for multiple scattering and self shielding: This correction has been determined by the Monte Carlo code SESH (Ref. 16) and the respective values are listed in Table III. The corrections are ∿ 2 % except for ^{197}Au, where corrections up to 6 % were calculated.

7. Correction for gamma-ray self-absorption:
In 2 Ref. 2 the calculated correction for gamma-ray self-absorption in a 1 mm thick gold sample was SA = 0.96 using the total energy absorption cross section given in Ref. 17. In order to check this calculation we measured the gamma-ray self-absorption by comparison of the capture yield from gold samples of variable thickness. Extrapolation of these yields to sample thickness zero provided a direct measure of the gamma-ray self-absorption. For a sample thickness of 1 mm we obtained in this way SA = 0.95, which is in a good agreement with the calculation mentioned above. Therefore, we adopted an average value SA = 0.955 for the self-absorption correction in the gold sample. For the ^{243}Am sample we calculated

the correction SA = 0.985 with the same procedure as is described for ^{241}Am in Ref. 2.

8. Influence of lead shieldings in front of the Moxon-Rae detectors.

The influence of the lead shieldings in front of the Moxon-Rae detectors was studied in a separate measurement where we determined the capture yield from an ^{238}U sample relative to a ^{197}Au sample for all lead absorbers. The result is given in Table IV. Within the accuracy of the measurement of ∿ 0.3 - 0.4 %, the thickness of the lead absorbers had no effect on the measured ratio. As the capture gamma-ray spectra of ^{238}U and ^{243}Am are very similar (see subsection 10 below) this result was assumed to hold for ^{243}Am also. Therefore, no correction was applied for this effect.

9. Dead time correction:

Due to the high background from the radioactivity of the ^{243}Am sample, the dead time for measurements with the sample and the reference sample is slightly different. But as most of the observed counting rate is due to the prompt gamma-ray peak (see Figs. 2,3) this effect is rather small. The dead time difference was determined to 0.03 %, 0.28 %, 0.8 % and 2.16 % for lead shieldings of 2.0, 1.0, 0.7, 0.5 cm thickness, respectively (Run I to IV). Therefore, no correction was applied in measurements with the two thicker absorbers, while the data taken with the thinner lead shieldings were corrected by the factors given above.

10. Correction for detector efficiency

As the capture gamma-ray spectra of sample and reference sample have not the same shape, deviations of the detector efficiency from the ideal shape may cause a systematic effect in relative measurements. The respective corrections were evaluated in Refs. 15 and 18 using (i) capture gamma-ray spectra calculated according to the statistical model and (ii) a shape of the efficiency versus gamma-ray energy as evaluated from literature[19]. The so obtained correction factors, K, for ^{238}U and ^{241}Am relative to a gold standard are compiled in Table V for both converter types. Due to the high degree of similarily in nuclear structure of ^{241}Am and ^{243}Am the capture gamma ray spectra of both isotopes are also expected to be very similar[20]. Because the correction factors K depent only weakly on the respective gamma-ray sepctra it is certainly justified to use the same value of K in the present evaluation than for ^{241}Am. From Table V can be seen that no correction is required for the data measured with the bismuth-graphite converter while a correction of $\sim$ 3 % is necessary for the measurements with the graphite converter. In Table V the K-values for a relative measurement $^{238}U/^{197}Au$ have been included for two reasons: (i) to demonstrate that the K-values are indeed insensitive to small differences of the capture gamma-ray spectra (in this case of ^{238}U and ^{241}Am) and (ii) to check the calculation of K-values by the results of the measurements given in Table IV. The K-values in Table V predict, that the ratio of the count rates in a $^{238}U/^{197}Au$ measurement are higher by 2.5 % if a graphite converter is

used instead of a bismuth-graphite converter. The experiment shows a difference of 2.3 % in very good agreement with this prediction.

Finally, the capture cross section ratio can be calculated by the equation:

$$\frac{\sigma_{\gamma,Am}}{\sigma_{\gamma,Au}} = \frac{C_{Am}}{C_{Au}} \cdot \frac{(MS*SS)_{Au}}{(MS*SS)_{Am}} \cdot \frac{SA_{Au}}{SA_{Am}} \cdot \frac{N_{Au}}{N_{Am}} \quad \frac{B_{Au}}{B_{Am}} \quad K$$

where

C = experimental counting rates, normalized to equal neutron fluence, corrected for the various background components and also for the influence of fission events and dead time;

$(MS*SS)_i$ and SA_i = corrections for multiple scattering, self-shielding, and gamma-ray self absorption;

N_i = sample thickness;

B_i = neutron separation energies and

K = efficiency correction.

III.B. Fission Cross-Section Measurements

The fission neutron spectra were evaluated in the same way as described in Refs. 2 and 3. In order to improve the statistical accuracy the spectra of Run I,II, III, IV (flight path 53 mm) and the spectra of Run V, VI (flight path 71 mm) were added. The experimental signal-to-background ratio is demonstrated in Fig. 4.

After subtraction of time-dependent and time-independent backgrounds an additional background component due to incomplete pulse shape discrimination of the capture gamma-rays had to be taken into account. The respective correction was calculated from the spectra measured with the gold sample which were normalized by means of the capture cross section ratio of ^{243}Am and gold as determined with the Moxon-Rae detectors. This normalization was performed in that high energy interval in the TOF spectra close to the prompt gamma-ray peak where only capture gamma-rays but no fission neutrons are recorded due to the approximate 18 ns mean flight time of the fission neutron between the sample and the detectors (see Ref.3). After unfolding the time distribution of the fission neutrons from the background subtracted spectra these were corrected for fission in ^{239}Pu. As mentioned already, an impurity of 0.03 % ^{239}Pu resulted from the decay of ^{243}Am in the 3.3 years since the last plutonium separation. The respective correction caused a reduction of the measured effect by $\sim$ 4 %.

The fission cross section ratio was determined according to the relation

$$\frac{\sigma_{f,Am}}{\sigma_{f,U}} = \frac{C_{Am}}{C_U} \cdot \frac{N_U}{N_{Am}} \cdot \frac{\bar{\nu}_U}{\bar{\nu}_{Am}} \cdot \frac{f_U}{f_{Am}} \cdot \frac{(MS*SS)_U}{(MS*SS)_{Am}}$$

where

U and Am = ^{235}U and ^{243}Am, respectively

C_i = counting rates in the TOF spectra

N_i = numbers of atom per barn

f_i = fractions of fission neutrons above the experimental threshold

Because no experimental information was available from literature, a value $\bar{\nu}_{Am} = 3.2 \pm 0.1$ was estimated from the known $\bar{\nu}$-values of $^{241,242}Am$, leading to a ratio $\bar{\nu}_U/\bar{\nu}_{Am} = 0.753$. For the ratio of fissions neutrons above the experimental threshold we used the same value $f_U/f_{Am} = 0.90$ as quoted for ^{241}Am in Ref. 3. The values MS*SS for multiple scattering and self-shielding are those of Table III.

IV RESULTS

As can be seen from Table II, the ratios of the capture and fission cross sections of ^{243}Am versus ^{197}Au and ^{235}U have been measured in eight different runs. Six runs were performed in the energy range from 5 to 100 keV and two runs in the range from 40 to 250 keV. In the capture measurements two independent results were obtained as Moxon-Rae detectors with two different converters were used simultaneously.

IV.A. Capture Cross Section

In Tables VI to XIII the resulting cross section ratios σ_γ (^{243}Am)/σ_γ(^{197}Au) are compiled in great detail: for each run the results of both detectors are quoted together with their respective average. The total uncertainty is dominanted by systematic uncertainties which are 3 - 4 % for most of the data points, but increase up to ∿ 15 - 25 % at very low energies. For easier judgement of this large amount of data Table XIV lists the average values of all data given in Tables VI to XIII. By comparison of all these results the following conclusions can be drawn: No systematic difference shows up between the results obtained

with different detectors (Runs I - VI). This in an important check for the reliability of the efficiency correction. The data derived from runs with different lead shieldings or flight paths deviate from their mean (Table XIV) by only ± 1.3 % on the average. These small differences can well be understood by the systematic uncertainties of background subtraction as discussed in Sec. V. In the high energy runs a systematic difference of ∿ ± 4 % is observed for the results with different detectors. This relatively large discrepancy can again be explained by the uncertainties due to background subtraction and by the statistics as in these runs the effect-to-background ratio is rather small (see Fig. 3b).

In Fig. 5 the experimental ratios have been converted to absolute cross sections using the ENDF/B-V cross section for the gold reference sample. In order to avoid confusion all data measured at a particular flight path but with different lead shieldings and converter materials are averaged according to their statistical uncertainties. The plotted error bars represent only the uncertainty of the experimental cross section ratio. The total uncertainty of most of the data points is 3 - 6 % in the energy range from 15 to 160 keV and increases up to 9 % at higher and up to 20 % at lower energies. The total uncertainty is dominanted by systematic uncertainties. The statistical accuracy is better than 1 % for energies between 20 and 80 keV and better than 3 % for all other energies except those points below 10 keV. No systematic differences were found between the data measured at different flight paths again confirming the reliability of the background corrections. This is further more supported by the fact that the high

energy data fit smoothly to the values in the low energy range. The numerical values for the absolute cross section are given in Tables XV to XVII.

As no other experimental data exist in the energy range of the present measurement, a comparison can be made only to predictions from model calculations. It can be seen from Fig. 5 that good agreement is found with the KEDAK evaluation[21] and the calculations of Mann and Schenter[22] which both were performed prior to the present measurement. The data listed in ENDF/B-V are lower by ∿ 20-30 %. The yet preliminary data of the UKNDL evaluation[23] is higher by ∿ 20 - 30 %. It has to be mentioned that recently Macklin revised his measurement of the gold capture cross section[24]. As the ENDF/B-V evaluation is mainly based on this experiment this would imply that the values given in Fig. 5 have to be lowered by ∿ 9 % at 5 keV, 3.3 % at 10 keV and 1 % at 30 keV.

IV.B. Fission Cross Section

The results for the fission cross section ratio of ^{243}Am versus ^{235}U are given in Table XVIII and Fig. 6. The experimental ratios are converted into absolute values using the ^{235}U fission cross section as recommended in Ref. 25. The data from Runs I, II, III, IV and from Runs V, VI have been combined to common data sets. The overall accuracy of 8 - 10 % is dominated by systematic uncertainties. In the region of overlap between 30 and 100 keV reasonable agreement is found between the low energy and the high energy runs. This is insofar remarkable as the signal-to-background ratio of the high energy runs is very poor in this energy range and thus this consistency again confirms the reliability of the background sub-

traction. In the energy range of the present experiment no other experimental data are available until now, except for the two lowest data points quoted in a preliminary publication of Behrens and Browne.[26] These results which were skipped in their final publication[27] are in good agreement with the present measurement, which thus extends the data of Behrens and Browne smoothly to lower energies, where the cross section is so small that measurements with ionisation chambers are increasingly difficult.

V. DISCUSSION OF UNCERTAINTIES

The systematic uncertainties of the adopted experimental method have been discussed in great detail in Refs. 2,3,9,10 and 11. Therefore it is here sufficient to concentrate on the essential assumptions which were used to evaluate the uncertainties of the present measurement. The various uncertainties were added quadratically and the resulting sums are quoted in Tables VI to XIII and XVIII.

V.A. Capture Cross-Section

1. Sample mass: An uncertainty of 1.5 % had to be assigned to the sample mass. This uncertainty is caused by the fact that part of the sample material might have been converted from AmO_2 to Am_2O_3 during the sintering process. The weight of the pellet given in Table I was determined after sintering. Therefore, a chemical composition of $AmO_{1.75}$ was assumed that yields an uncertainty of 1.5 % for the mass. Thus, both compositions AmO_2 and Am_2O_3 are possible within the quoted uncertainty.

2. Flight path and time-dependent background: To evaluate these effects for sample and reference sample, an uncertainty of 0.3 mm was assumed for the measured flight paths. This gives rise to an uncertainty in the transformation of the individual spectra to a common flight path that consists of two components - an uncertainty in solid angle and an uncertainty in the transformation of the time scale.
The improved method to determine the flight path allowed for a higher accuracy compared to previous measurements (Ref. 2,9).

3. Constant background: This correction was calculated in the same way as described in Ref. 9.

4. Fission events: An overall uncertainty of 15 % was obtained for this correction which is composed of the following parts: Neglection of the unfolding procedure caused an uncertainty of 10 % which is the average difference of the results for the fission cross section obtained with and without unfolding procedure. An uncertainty of 5 % was assumed for the ratio f_U/f_{Am} of fission neutrons above the detector threshold (see Sec. III B) while the $\bar{\nu}$ values were taken with an uncertainty of 3.3 % and 1 % for ^{243}Am and ^{235}U, respectively. An additional uncertainty of 10 % was caused by the differecne in total fission gamma-ray energy of ^{243}Am and ^{235}U.

5. Multiple scattering and self-shielding. The uncertainty of this correction was calculated in the same way as described in Ref. 9. A value of 1.4 % was found for the ratio $(MS*SS)_{Au}/(MS*SS)_{Am}$.

6. Neutron fluence: By means of the two additional lithium glass detectors located at 0° and 20° with respect to the beam axis it could be verified that sample and reference sample were exposed to the same neutron fluence within 0.5 %.

7. Gamma-ray self-absorption: The good agreement of calculated and measured gamma-ray self-absorption factors for the gold sample showed that the ratio SA_{Au}/Sa_{Am} is correct within an uncertainty of 1 %.

8. Lead shielding in front of the Moxon-Rae detectors: From the numbers given in Table IV we deduced a systematic uncertainty of 0.3 % for this effect.

9. Dead time correction. As this correction was very small and could be determined with high accuracy the related systematic uncertainty was neglected.

10. Detector efficiency: The accuracy of the efficiency corrections was carefully studied in Refs. 18 and 28 using different efficiency curves and different capture gamma-ray spectra for the gold sample. As a result, an accuracy of 1.2 % can be assigned to the correction factor K. This high precision is confirmed by the fact that no difference could be observed in the final cross section ratios measured with different converter materials (see Table XIV).

V.B. Fission Cross Section

The systematic uncertainties due to sample mass, flight path, time-dependent and time-independent background were evaluated in the same way as described for the capture cross-section measurements. The remaining effects are:

1. Unfolding procedure: The systematic uncertainty for the unfolding of the fission neutron time distribution varied between 4 and 6 %. These values account for 50 % of the difference in the cross section ratio, if the evaluation is made with and without unfolding procedure.

2. Isotopic impurities: Contrary to the capture rate the effect of isotopic impurities could not be neglected for the fission cross section. On the average the correction for fission in ^{239}Pu amounted to $\sim$ 4 % of the measured effect, thus contributing an uncertainty of less than 1 % to the cross section ratio, if a 20 % accuracy is assumed for the estimated ^{239}Pu content. After the measurements the ^{243}Am sample was analysed by X-ray absorptiometry[29]. The observed effect in the region of the K-absorption edge of plutonium is shown in Fig. 7 together with the 2σ band of the statistical accuracy. A possible plutonium contamination of 0.2 % would have shown up as indicated by the dashed-dotted line. It is confirmed that the plutonium contamination is less than 0.06 % on a 1σ confidence level. This is in agreement with the assumption that plutonium was completely removed in the purification of the material 3 years before our measurement.

   The analysis, however, indicated a contamination of uranium, in contrast to the analysis provided by the owner of the material. This contamination was determined to 0.18 $\pm$ 0.02 % by means of the more sensitive method of X-ray fluorescence[29]. This method was applicable for uranium (but not for plutonium) as no uranium X-rays occur in the decay of the sample material itself.

As it is very unlikely that this uranium is highly enriched in ^{235}U, this contamination will not affect the fission cross section measurement. Nevertheless, an isotopic analysis is presently underway.

3. Background due to the incomplete gamma discrimination: The background caused by capture gamma-rays which were not rejected by the pulse shape discriminator could be determined with an accuracy of ∿ 30 %.

4. Fraction of fission neutrons above threshold. In Refs. 2 and 3 the respective correction for ^{241}Am was estimated to ∿ 3 - 4 %. In the present experiment the same value f_U/f_{Am} was used for ^{243}Am assuming a somewhat larger uncertainty of 5 %.

5. Average number of fission neutrons: An uncertainty of 3.3 % was assumed for the estimated $\bar{\nu}$ value of ^{243}Am, while the respective value for ^{235}U was taken to be correct within 1 %.

6. Multiple scattering and neutron fluence: These uncertainties are the same as for the capture measurement.

7. Angular distribution of fission neutrons: This correction was discussed in detail for the ^{241}Am measurement in Refs. 2 and 3 with the conclusion that no correction was required. The same assumption was made for the present measurement.

V. C. Conversion of Experimental Ratios to Absolute Values

Both reference cross sections ^{197}Au and ^{235}U exhibit a distinct structure in the energy range of the present measurements. It was pointed out by Liskien and Weigmann[30] that a systematic uncertainty arises if smoothed reference cross sections are used for converting the measured ratios to absolute cross sections.

In the present experiment the high resolution cross section for gold was taken from ENDF/B-V to convert the data to absolute cross sections. The values of $\sigma_\gamma(^{197}Au)$ given in Tables XV - XVII are averages over the energy interval of each data point. It should be noted again that the gold cross section of ENDF/B-V probably has to be changed as the data of Macklin et al. have been revised recently (Ref. 24). In case of ^{235}U fission a smooth cross section (as recommended in Ref. 25) was used for the conversion. This might be acceptable as the structure is less pronounced than the one in the gold capture cross section. Moreover, the present fission cross section is dominated by other uncertainties.

VI. CONCLUSIONS

For the first time the capture and fission cross sections of ^{243}Am have been determined in the energy range from 5 to 250 keV. The measurements cover most of the neutron energy range of interest for fast reactors, where data are requested urgently. The experimental method applied offered a high neutron flux at the sample position thus allowing for a signal-to-background ratio of 1 or even better in spite of the high radioactivity of the sample material. Consequently, data could be recorded with high statistical

accuracy (1-3 % for most of the data points) in a measuring time of ∿ 1 to 2 days. The overall accuracy of better than 5 % for capture and ∿ 10 % for fission is sufficient to meet all data requests (Refs. 5,6,7,8).

For the example of the capture cross section Fig. 5 illustrates impressively the capabilities of present theoretical model calculations. If important model parameters, like D_{OBS} and Γ_{γ}, are known from the resonance region, the calculations can predict the cross sections with an accuracy of ∿ 10 %. On the other hand oversimplified calculations with global parameters are insufficient to meet the requirements.

A final remark may be added concerning the virtues and potentials of our experimental technique. One important and somewhat unexpected feature of the present method to determine capture cross sections was that it proved to be very insensitive to a lead shielding in front of the detectors. Even with 2 cm of lead a high statictical accuracy was obtained in a measuring time of only 6 h per sample. Thus, one may think of capture cross section measurements on even more radioactive actinides or fission products keeping in mind that a further reduction of the flight path and hence a correspondingly higher neutron flux at the sample position is still possible. The main problem for measurements on such exotic isotopes may, however, be to get suitable samples.

ACKNOWLEDGEMENTS

We would like to thank J. F. Gueugnon from the EURATOM Institute for Transuranium Elements for the preparation of the ^{243}Am sample. Thanks are also due to H. Ottmar for the X-ray analyses and E. Mainka for the isotopic analyses of the sample material. We appreciated very much the help of G. Reffo in estimating the capture gamma ray spectrum of ^{243}Am. The measurements were only possible through the continuous support of A. Ernst and D. Roller in providing optimum beam conditions and the help of G. Rupp in optimizing the experimental setup. Finally, we would like to acknowledge the support of the U.S. Department of Energy in making available the sample material.

REFERENCES

1.) K. WISSHAK, F. KÄPPELER and F.H. FRÖHNER
Proc. of the IAEA Consultants Meeting on Uranium and Plutonium Isotope Resonance Parameters Vienna 28. September to 2. October 1981 INDC(NDS)-129/GJ. International Atomic Energy Agency, Vienna 1982

2.) K. WISSHAK and F. KÄPPELER, Nucl. Sci. Eng. 76, 148 (1980)

3.) W. HAGE, K. WISSHAK and F.KÄPPELER,
Nucl. Sci. Eng. 78, 248 (1981)

4.) H.H. KNITTER and C. BUDTZ - JØRGENSEN
Atomkernenergie - Kerntechnik, 33, 205 (1979)

5.) B.H. PATRICK and M.G. SOWERBY, "U.K. Nuclear Data Progress Report 1979", UKNDC (80) P 96,
NEANDC (E) 212 Vol. 8, INDC (UK) - 32)/LN
United Kingdom Atomic Energy Authority Harwell 1980

6.) N. DAYDAY, Ed. "World Request List for Nuclear Data",
INDC (SEC) - 78 / URSF
International Atomic Energy Agency, Vienna 1981

7.) J. BOUCHARD Proc. of the Second Advisory Group Meeting in Transactinium Isotope Nuclear Data Cadarache 2 - 5 May 1979
IAEA-TECDOC - 232 International Atomic Energy Agency 1980 p.1

8.) H. KOUTS Proc. of the Second Advisory Group Meeting on Transactinium Isotope Nuclear Data Cadarache 2-5 May 1979
IAEA-TECDOC - 232 International Atomic Energy Agency 1980 p.23

9.) K. WISSHAK and F. KÄPPELER, Nucl. Sci. Eng. 66, 363 (1978)

10.) K. WISSHAK and F. KÄPPELER, Nucl. Sci. Eng. 69, 39 (1979)

11.) K. WISSHAK and F. KÄPPELER, Nucl. Sci. Eng. 69, 47 (1979)

12.) K. WISSHAK, F. KÄPPELER, G. REFFO, and F. FABBRI,
Proc. of the NEANDC/NEACRP Specialists Meeting on Fast Neutron Capture Cross Sections Argonne National Laboratory 20 - 23 April 1982 to be published

13.) K. WISSHAK and F. KÄPPELER, Proc. of Int. Conf. on Nuclear Data for Science and Technology Antwerp 6-10 Sept. 1982 to be published

14.) R.L. MACKLIN, J.H. GIBBONS, and T. INADA,
Nucl. Phys. 43, 353 (1963)

15.) K. WISSHAK, J. WICKENHAUSER, F.KÄPPELER, G. REFFO, and F. FABBRI, Nucl. Sci. Eng. 81 396 (1982)

16.) F. H. FRÖHNER, "SESH-A Fortran IV Code for Calculating the Self-Shielding and Multiple Scattering Effects for Neutron Cross Section Data Interpretation in the Unresolved Resonance Region, "GA-8380, Gulf General Atomic (1968)

17.) E. STORM and H.I. ISRAEL, Nucl. Data Tables A, 7, 565 (1970)

18.) G. REFFO, F. FABBRI, K. WISSHAK, and F. KÄPPELER
Nucl. Sci. Eng. in print (manuscript No 43-82N)

19.) K. WISSHAK and F.KÄPPELER, Nucl. Sci. Eng. 77, 58 (1981)

20.) G. REFFO, private communications 1982

21.) F.H. FRÖHNER, B. GOEL, U. FISCHER and H. JAHN
Proc. of Int. Conf. on Nuclear Data for Science and Technology Antwerp 5-10 Sept. 1982, to be published

22.) F.M. MANN and R.E. SCHENTER
Nucl. Sci. Eng. 63, 242 (1977)

23.) B. PATRICK et al. UKNDL - Evaluation
private communications 1982

24.) R.L. MACKLIN private communications 1982

25.) W.P. POENITZ and A.B. SMITH, Eds., Proc. NEANDC/NEACRP Specialists Mtg. Fast Neutron Cross Sections of ^{233}U, ^{235}U, ^{238}U, and ^{239}Pu, Argonne, Illinois, June 28-30, 1976, CONF-760647, ANL-76-90, ERDA-NDC-5/L, NEANDC(US)-199/L, Suppl. p. 29, Argonne National Laboratory (1976)

26.) J.W. BEHRENS "Measurement of the Neutron-Induced Fission Cross Section of ^{243}Am Relative to ^{235}U from 0.1 MeV to 30 MeV", UCID-17504 Lawrence Livermore Laboratory 1977

27.) J.W. BEHRENS and J.C. BROWNE, Nucl. Sci. Eng. 77, 444 (1981)

28.) G. REFFO, F. FABBRI, K. WISSHAK and F. KÄPPELER
Nucl. Sci. Eng. 80, 630 (1982)

29.) H. OTTMAR, H. EBERLE, P. MATUSSEK, I. MICHEL-PIPER,
Proc. of Int. Symp. on Recent Advances in Nuclear Materials Safeguards, IAEA-SM-260/34
International Atomic Energy Agency to be published

30.) H. LISKIEN and H. WEIGMANN, Ann. Nucl. Energy 4, 38 (1977)

Table I Compilation of the Relevant Sample Data

Sample Number	Sample	Chemical Composition	Isotopic Composition	Weight (g)	Thickness (atom/b)	Thickness (mm)	Diameter (mm)
1	^{243}Am	$Am\ O_{1.75}$ sintered pellet	99.82 % ^{243}Am 0.17 % ^{241}Am 0.01 % ^{244}Cm	0.970	$1.400 \cdot 10^{-3}$	0.9	14
2	^{197}Au	Metal (99.9 %)	Natural	2.936	$5.832 \cdot 10^{-3}$	1.0	14
3	C	Graphite	Natural	0.256	$8.339 \cdot 10^{-3}$	0.7	14
4	^{235}U	Metal	0.758 % ^{234}U 92.91 % ^{235}U 0.266 % ^{236}U 6.064 % ^{238}U	1.624	$2.520 \cdot 10^{-3}$ ^{235}U	0.7	14

Table II Parameters for the Individual Measurements of the Neutron Capture Cross Section Ratio $\sigma_\gamma(^{243}Am)/\sigma_\gamma(^{197}Au)$

Run Number	Lead Shielding of Moxon-Rae Detectors (cm)	Flight Path (mm)	Evaluated Neutron Energy Range (keV)	Measuring Time per Sample (h)
I	2.0	52.7	5 - 90	9.6
II	1.0	52.9	5 - 90	8.5
III	0.7	52.2	5 - 90	7.5
IV	0.5	53.2	5 - 90	8.1
V	2.0	70.8	7 - 90	25.8
VI	1.0	71.4	7 - 90	21.2
VII	2.0	52.4	30 - 250	27.1
VIII	2.0	65.1	40 - 250	24.7

Table III Correction Factors for Multiple Scattering, Self-Shielding and Gamma-Ray Self-Absorption in the Samples

Sample Number	Sample	Energy (keV)	Multiple Scattering (MS)	Self-Shielding (SS)	Total (MS x SS)	Gamma-Ray Self-Absorption (SA)
1	^{243}Am	5 - 320	1.040	0.984	1.023	0.985
2	^{197}Au	5	1.121	0.872	0.977	0.955
		10	1.118	0.919	1.027	
		20	1.113	0.946	1.053	
		40	1.099	0.960	1.055	
		80	1.100	0.965	1.062	
		160	1.069	0.975	1.042	
		320	1.066	0.975	1.039	
4	^{235}U	5 - 320	1.04	0.99	1.025	

Table IV — Intensity ratio of capture gamma-rays measured from a ^{238}U and a ^{197}Au sample for different lead absorbers (the statistical uncertainty is given in brackets).

Thickness of Lead Absorber (cm)	Count Rate Ratio $^{238}U/^{197}Au$	
	Graphite Converter (rel units)	Bismuth-Graphite Converter (rel units)
2	2.607 (0.53 %)	2.560 (0.49 %)
1	2.598 (0.41 %)	2.559 (0.41 %)
0.7	2.599 (0.44 %)	2.547 (0.41 %)
0.5	2.613 (0.29 %)	2.556 (0.27 %)
0	2.617 (0.27 %)	2.544 (0.26 %)
weighted average	2.609 (0.16 %)	2.551 (0.15 %)

Table V Correction factors K for relative measurements using a gold standard and Maxon-Rae detectors with different converters

Cross Section Ratio	Correction Faktor K	
	Graphite Converter	Bismuth-Graphite Converter
$^{241}Am/^{197}Au$	0.973	1.000
$^{238}U/^{197}Au$	0.972	0.996

Table VI Experimental Results for the Neutron Capture Cross Section of ^{243}Am Relative to ^{197}Au
Run I: Flight Path 52.7 mm; Lead Shielding 2.0 cm; Maximum Neutron Energy 90 keV

En ± ΔEn (keV)		Bismuth-Graphite Converter			Graphite Converter			Average			
		$\frac{\sigma_\gamma(^{243}Am)}{\sigma_\gamma(^{197}Au)}$	Uncertainty (%) Statistical	Systematic	$\frac{\sigma_\gamma(^{243}Am)}{\sigma_\gamma(^{197}Au)}$	Uncertainty (%) Statistical	Systematic	$\frac{\sigma_\gamma(^{243}Am)}{\sigma_\gamma(^{197}Au)}$	Uncertainty (%) Statistical	Systematic	Total
5.7	0.8	2.40	17.2	13.0	2.00	20.0	13.8	2.19	13.0	13.4	18.7
7.5	1.1	2.05	12.2	9.0	2.40	12.2	8.6	2.20	8.6	8.8	12.7
10.1	1.7	2.44	7.7	6.4	2.65	7.4	6.0	2.54	5.3	6.2	8.2
12.9	1.4	2.68	7.4	5.0	2.68	7.7	5.1	2.69	5.3	5.1	7.4
15.7	1.8	3.00	4.7	4.2	2.75	5.5	4.4	2.88	3.6	4.3	5.6
18.3	1.0	3.14	5.2	4.0	3.05	5.7	4.1	3.10	4.0	4.1	5.7
20.6	1.2	3.06	4.7	4.0	3.16	5.0	4.0	3.10	3.4	4.0	5.3
23.2	1.4	3.35	3.6	3.8	3.40	4.0	3.9	3.37	2.7	3.9	4.7
26.4	1.7	3.35	2.9	3.4	3.35	3.1	3.4	3.35	2.1	3.4	4.0
30.2	2.0	3.44	2.4	3.4	3.26	2.5	3.3	3.35	1.7	3.4	3.8
35.0	2.5	3.51	2.0	3.4	3.54	2.2	3.3	3.52	1.5	3.4	3.7
41.1	3.0	3.53	1.8	3.2	3.58	1.9	3.2	3.56	1.3	3.2	3.5
48.8	3.9	3.75	1.6	3.2	3.82	1.7	3.2	3.79	1.2	3.2	3.4
59.0	5.0	3.82	1.4	3.2	3.78	1.5	3.2	3.80	1.0	3.2	3.4
72.8	6.7	3.73	1.4	4.0	3.79	1.5	4.0	3.76	1.0	4.0	4.1
92.1	9.2	3.39	2.7	9.9	3.62	3.5	9.5	3.47	2.1	9.7	9.9

Table VII Experimental Results for the Neutron Capture Cross Section of ^{243}Am Relative to ^{197}Au

Run II: Flight Path 52.9 mm; Lead Shielding 1.0 cm; Maximum Neutron Energy 90 keV

En ± ΔEn (keV)		Bismuth-Graphite Converter			Graphite Converter			Average			
		$\frac{\sigma_\gamma(^{243}Am)}{\sigma_\gamma(^{197}Au)}$	Uncertainty (%)		$\frac{\sigma_\gamma(^{243}Am)}{\sigma_\gamma(^{197}Au)}$	Uncertainty (%)		$\frac{\sigma_\gamma(^{243}Am)}{\sigma_\gamma(^{197}Au)}$	Uncertainty (%)		
			Statistical	Systematic		Statistical	Systematic		Statistical	Systematic	Total
5.7	0.8	1.13	37.9	34.0	2.77	22.5	20.7	1.66	21.3	25.7	33.3
7.5	1.1	1.47	16.7	14.9	2.39	17.3	15.8	1.71	12.3	15.3	19.6
10.2	1.7	2.30	6.8	7.1	2.55	10.3	10.0	2.36	5.7	8.3	10.1
13.1	1.4	2.48	6.1	5.3	2.56	8.7	6.6	2.50	5.0	5.8	7.7
15.9	1.8	3.03	3.6	4.3	3.03	5.6	5.1	3.03	3.0	4.6	5.5
18.6	1.0	2.93	3.8	4.0	3.01	5.9	4.5	2.95	3.2	4.2	5.3
20.9	1.2	3.27	3.1	4.0	3.37	4.6	4.2	3.30	2.6	4.1	4.9
23.5	1.4	3.26	2.4	3.9	3.34	3.7	4.0	3.28	2.0	4.0	4.5
26.8	1.7	3.40	2.0	3.4	3.27	2.9	3.5	3.36	1.6	3.5	3.9
30.7	2.0	3.33	1.7	3.3	3.46	2.2	3.4	3.38	1.3	3.4	3.6
35.6	2.5	3.48	1.4	3.3	3.51	2.0	3.3	3.49	1.1	3.3	3.5
41.8	3.1	3.58	1.2	3.3	3.57	1.7	3.3	3.58	1.0	3.3	3.5
49.7	4.0	3.65	1.2	3.3	3.63	1.6	3.3	3.64	1.0	3.3	3.5
60.0	5.2	3.69	1.1	3.3	3.79	1.5	3.3	3.72	0.9	3.3	3.4
74.0	6.8	3.61	1.2	4.6	3.74	1.5	4.5	3.66	0.9	4.6	4.7
93.5	9.4	3.25	2.6	9.7	3.59	3.3	9.3	3.36	2.0	9.5	9.7

Table VIII Experimental Results for the Neutron Capture Cross Section of ^{243}Am Relative to ^{197}Au
Run III: Flight Path 52.2 mm; Lead Shielding 0.7 cm; Maximum Neutron Energy 90 keV

En ± ΔEn (keV)		Bismuth-Graphite Converter			Graphite Converter			Average			
		$\frac{\sigma_\gamma(^{243}Am)}{\sigma_\gamma(^{197}Au)}$	Uncertainty (%) Statistical	Systematic	$\frac{\sigma_\gamma(^{243}Am)}{\sigma_\gamma(^{197}Au)}$	Uncertainty (%) Statistical	Systematic	$\frac{\sigma_\gamma(^{243}Am)}{\sigma_\gamma(^{197}Au)}$	Uncertainty (%) Statistical	Systematic	Total
5.6	0.8	1.89	22.4	26.0	1.55	47.0	21.3	1.81	20.2	24.4	31.7
7.3	1.1	1.81	13.5	15.8	1.95	22.0	10.8	1.85	11.5	13.9	18.0
9.9	1.7	2.52	6.2	8.1	2.28	12.2	7.0	2.46	5.5	7.7	9.5
12.7	1.4	2.65	5.5	5.7	2.46	10.3	5.1	2.60	4.9	5.5	7.4
15.5	1.8	2.82	3.9	4.7	2.79	6.8	4.4	2.82	3.4	4.6	5.7
18.0	1.0	2.98	3.9	4.2	2.70	7.4	4.1	2.91	3.5	4.2	5.5
20.2	1.2	3.32	3.2	4.0	3.18	5.5	3.9	3.28	2.8	4.0	4.9
22.9	1.4	3.43	2.5	3.8	3.29	4.2	3.8	3.39	2.1	3.8	4.3
26.0	1.7	3.38	2.0	3.5	3.31	3.2	3.4	3.36	1.7	3.5	3.9
29.9	2.0	3.40	1.6	3.4	3.36	2.6	3.4	3.39	1.4	3.4	3.7
34.7	2.5	3.66	1.4	3.4	3.57	2.1	3.4	3.63	1.2	3.4	3.6
40.8	3.0	3.68	1.2	3.3	3.79	1.8	3.4	3.71	1.0	3.4	3.5
48.6	3.9	3.74	1.1	3.3	3.67	1.7	3.4	3.72	0.9	3.4	3.5
58.8	5.0	3.86	1.0	3.3	3.81	1.5	3.3	3.84	0.8	3.3	3.4
72.6	6.7	3.78	1.0	4.1	3.86	1.5	4.1	3.81	0.8	4.1	4.2
91.9	9.2	3.52	1.8	9.2	3.63	3.3	8.9	3.54	1.6	9.1	9.2

Table IX Experimental Results for the Neutron Capture Cross Section of ^{243}Am Relative to ^{197}Au

Run IV: Flight Path 53.2 mm; Lead Shielding 0.5 cm; Maximum Neutron Energy 90 keV

En ± ΔEn (keV)		Bismuth-Graphite Converter			Graphite Converter			Average			
		$\frac{\sigma_\gamma(^{243}Am)}{\sigma_\gamma(^{197}Au)}$	Uncertainty (%)		$\frac{\sigma_\gamma(^{243}Am)}{\sigma_\gamma(^{197}Au)}$	Uncertainty (%)		$\frac{\sigma_\gamma(^{243}Am)}{\sigma_\gamma(^{197}Au)}$	Uncertainty (%)		
			Statistical	Systematic		Statistical	Systematic		Statistical	Systematic	Total
5.8	0.8	1.69	26.9	26.5	0.57	154.0	177.0	1.45	27.7	48.8	56.1
7.6	1.1	1.89	15.8	16.0	1.53	38.0	43.6	1.82	14.6	24.1	28.2
10.3	1.7	2.64	7.0	7.9	2.31	15.0	17.5	2.57	6.3	10.9	12.6
13.1	1.4	3.06	5.9	5.5	2.37	16.7	11.3	2.94	5.6	7.0	9.0
15.9	1.8	2.95	4.3	4.7	2.81	8.5	7.5	2.92	3.8	5.6	6.8
18.5	1.0	3.11	4.5	4.3	3.42	7.6	5.6	3.18	3.9	4.8	6.2
20.7	1.2	3.27	3.5	4.1	3.37	6.5	5.2	3.29	3.1	4.5	5.5
23.4	1.4	3.52	2.7	3.9	3.37	4.9	4.6	3.48	2.4	4.1	4.8
26.5	1.7	3.60	2.1	3.4	3.56	3.6	3.8	3.59	1.8	3.5	3.9
30.4	2.0	3.49	1.7	3.4	3.46	3.1	3.7	3.48	1.5	3.5	3.8
35.2	2.5	3.73	1.5	3.3	3.71	2.5	3.6	3.72	1.3	3.4	3.6
41.3	3.0	3.76	1.3	3.3	3.80	2.2	3.5	3.77	1.1	3.4	3.6
49.0	3.9	3.79	1.2	3.3	3.66	2.1	3.5	3.75	1.0	3.4	3.5
59.3	5.0	3.93	1.1	3.3	4.02	1.8	3.4	3.95	0.9	3.3	3.4
73.0	6.7	3.79	1.1	4.2	3.92	1.8	4.3	3.82	0.9	4.2	4.3
92.3	9.2	3.22	2.8	10.2	3.69	4.7	9.9	3.32	2.4	10.0	10.3

Table X Experimental Results for the Neutron Capture Cross Section of ^{243}Am Relative to ^{197}Au

Run V: Flight Path 70.8 mm; Lead Shielding 2.0 cm; Maximum Neutron Energy 90 keV

$\bar{E}n \pm \Delta En$ (keV)		Bismuth-Graphite Converter			Graphite Converter			Average			
		$\frac{\sigma_\gamma(^{243}Am)}{\sigma_\gamma(^{197}Au)}$	Uncertainty (%)		$\frac{\sigma_\gamma(^{243}Am)}{\sigma_\gamma(^{197}Au)}$	Uncertainty (%)		$\frac{\sigma_\gamma(^{243}Am)}{\sigma_\gamma(^{197}Au)}$	Uncertainty (%)		
			Statistical	Systematic		Statistical	Systematic		Statistical	Systematic	Total
7.0	0.8	2.71	22.7	10.1	2.40	25.0	10.9	2.55	16.8	10.5	19.8
8.7	1.1	2.68	21.4	9.9	2.33	18.2	8.3	2.45	13.9	9.0	16.6
11.1	1.6	2.37	13.3	6.7	2.41	12.7	6.3	2.39	9.2	6.5	11.3
13.5	1.2	3.07	12.1	4.9	3.00	10.9	4.6	3.03	8.0	4.7	9.3
15.7	1.4	2.93	9.6	4.3	2.75	9.2	4.3	2.84	6.6	4.3	7.9
17.6	0.7	2.65	10.8	3.9	3.37	9.1	3.7	2.98	7.0	3.8	8.0
19.1	0.8	2.96	9.2	3.7	3.57	8.0	3.5	3.25	6.1	3.6	7.1
20.8	0.9	3.69	7.1	3.5	3.18	7.5	3.6	3.41	5.2	3.6	6.3
22.8	1.0	3.29	5.9	3.3	3.22	5.9	3.4	3.25	4.2	3.4	5.4
25.0	1.2	3.33	5.1	3.4	3.30	5.1	3.3	3.31	3.6	3.4	5.0
27.7	1.3	3.21	4.1	3.1	3.45	3.8	3.1	3.33	2.8	3.1	4.2
30.7	1.5	3.57	3.5	3.1	3.38	3.5	3.0	3.47	2.5	3.1	4.0
34.2	1.7	3.67	3.2	3.0	3.61	3.3	3.0	3.64	2.3	3.0	3.8
38.4	2.1	3.61	2.7	3.0	3.43	2.8	3.0	2.52	1.9	3.0	3.6
43.5	2.4	3.61	2.1	3.0	3.83	2.6	3.0	3.69	1.6	3.0	3.4
49.5	2.9	3.77	2.4	3.0	3.69	2.5	3.0	3.73	1.7	3.0	3.5
56.9	3.8	3.95	2.2	3.0	3.71	2.3	3.0	3.83	1.6	3.0	3.4
66.2	4.4	3.75	2.2	3.0	3.80	2.1	3.0	3.78	1.5	3.0	3.4
77.9	5.5	3.80	2.4	3.8	3.85	2.4	3.7	3.82	1.7	3.8	4.2
93.1	7.0	3.45	4.4	7.8	3.49	4.4	8.1	3.47	3.1	8.0	8.6

Table XI Experimental Results for the Neutron Capture Cross Section of ^{243}Am Relative to ^{197}Au

Run VI: Flight Path 71.4 mm; Lead Shielding 1.0 cm; Maximum Neutron Energy 90 keV

$E_n \pm \Delta E_n$ (keV)	Bismuth-Graphite Converter			Graphite Converter			Average			
	$\frac{\sigma_\gamma(^{243}Am)}{\sigma_\gamma(^{197}Au)}$	Uncertainty (%)		$\frac{\sigma_\gamma(^{243}Am)}{\sigma_\gamma(^{197}Au)}$	Uncertainty (%)		$\frac{\sigma_\gamma(^{243}Am)}{\sigma_\gamma(^{197}Au)}$	Uncertainty (%)		
		Statistical	Systematic		Statistical	Systematic		Statistical	Systematic	Total
7.2 0.8	2.35	12.4	11.4	2.03	19.4	13.8	2.24	10.5	12.3	16.2
9.0 1.1	2.63	8.6	8.5	2.61	12.8	9.7	2.62	7.1	9.0	11.5
11.4 1.6	2.48	6.0	6.4	2.50	8.2	6.7	2.49	4.8	6.5	8.1
13.9 1.2	2.83	6.1	5.0	2.69	8.0	5.1	2.78	4.9	5.1	7.1
16.1 1.4	2.80	4.6	4.3	2.86	6.2	4.5	2.82	3.7	4.4	5.8
18.0 0.7	2.88	5.2	4.0	3.10	6.7	4.0	2.95	4.1	4.0	5.7
19.5 0.8	3.23	4.2	3.7	3.15	5.8	3.8	3.20	3.4	3.8	5.1
21.3 0.9	3.33	3.6	3.6	3.24	4.9	3.7	3.30	2.9	3.7	4.7
23.3 1.0	3.43	2.8	3.5	3.34	3.8	3.5	3.40	2.3	3.5	4.2
25.6 1.2	3.34	2.6	3.4	3.26	3.3	3.4	3.31	2.0	3.4	3.9
28.3 1.3	3.33	2.0	3.1	3.52	2.6	3.1	3.39	1.6	3.1	3.5
31.3 1.5	3.59	1.7	3.1	3.41	2.5	3.1	3.53	1.4	3.1	3.4
34.9 1.7	3.66	1.6	3.0	3.67	2.2	3.1	3.66	1.3	3.1	3.4
39.3 2.1	3.68	1.4	3.0	3.57	1.9	3.0	3.64	1.1	3.0	3.2
44.4 2.5	3.66	1.3	3.0	3.75	1.8	3.0	3.69	1.1	3.0	3.2
50.6 3.0	3.77	1.2	3.0	3.76	1.6	3.0	3.77	1.0	3.0	3.2
58.3 3.7	3.84	1.2	3.0	3.82	1.5	3.0	3.83	0.9	3.0	3.1
67.8 4.5	3.86	1.1	3.0	3.82	1.4	3.0	3.85	0.9	3.0	3.1
79.8 5.7	3.79	1.2	3.8	3.93	1.6	3.8	3.84	1.0	3.8	3.9
95.4 7.2	3.57	2.3	8.7	3.89	3.6	8.9	3.65	1.9	8.8	9.0

Table XII Experimental Results for the Neutron Capture Cross Section of ^{243}Am Relative to ^{197}Au

Run VII: Flight Path 52.4 mm; Lead Shielding 2.0 cm; Maximum Neutron Energy 250 keV

En ± ΔEn (keV)		Bismuth-Graphite Converter			Graphite Converter			Average			
		$\frac{\sigma_\gamma(^{243}Am)}{\sigma_\gamma(^{197}Au)}$	Uncertainty (%) Statistical	Systematic	$\frac{\sigma_\gamma(^{243}Am)}{\sigma_\gamma(^{197}Au)}$	Uncertainty (%) Statistical	Systematic	$\frac{\sigma_\gamma(^{243}Am)}{\sigma_\gamma(^{197}Au)}$	Uncertainty (%) Statistical	Systematic	Total
34.4	2.4	4.26	27.5	6.2	4.30	13.1	5.2	4.29	11.8	5.5	13.0
40.3	2.9	3.43	13.9	4.6	3.43	13.2	5.4	3.43	9.6	5.0	10.8
47.9	3.8	4.00	9.6	4.2	4.06	8.7	4.4	4.03	6.4	4.3	7.7
57.8	4.9	4.64	7.8	4.0	3.95	7.7	4.2	4.23	5.5	4.1	6.9
71.1	6.5	3.84	5.9	3.8	4.11	5.3	3.8	3.98	3.9	3.8	5.4
89.7	8.9	4.11	4.8	3.7	3.84	4.3	3.7	3.95	3.2	3.7	4.9
116.6	13.1	3.45	3.8	3.6	3.32	3.5	3.6	3.38	2.6	3.6	4.4
157.9	20.4	3.18	3.0	3.6	3.09	2.7	3.5	3.12	2.0	3.6	4.1
226.1	33.9	2.60	4.5	6.5	2.57	3.9	5.9	2.59	2.9	6.2	6.8

Table XIII Experimental Results for the Neutron Capture Cross Section of ^{243}Am Relative to ^{197}Au

Run VIII: Flight Path 65.1 mm; Lead Shielding 2.0 cm; Maximum Neutron Energy 250 keV

En ± ΔEn (keV)		Bismuth-Graphite Converter			Graphite Converter			Average			
		$\frac{\sigma_\gamma(^{243}Am)}{\sigma_\gamma(^{197}Au)}$	Uncertainty (%)		$\frac{\sigma_\gamma(^{243}Am)}{\sigma_\gamma(^{197}Au)}$	Uncertainty (%)		$\frac{\sigma_\gamma(^{243}Am)}{\sigma_\gamma(^{197}Au)}$	Uncertainty (%)		
			Statistical	Systematic		Statistical	Systematic		Statistical	Systematic	Total
38.2	2.2	2.93	27.0	5.6	4.19	21.8	4.5	3.47	17.2	5.0	17.9
43.7	2.7	3.50	18.9	4.5	4.31	22.6	4.7	3.76	14.6	4.6	15.3
50.3	3.3	4.24	16.3	4.3	3.41	16.4	4.0	3.73	11.6	4.2	12.3
58.7	4.1	3.86	12.4	3.8	3.78	13.8	3.9	3.83	9.2	3.9	10.0
69.2	5.1	4.19	10.4	3.6	3.94	9.3	3.4	4.04	6.9	3.5	7.7
83.0	6.6	4.39	7.9	3.4	4.07	7.7	3.3	4.21	5.5	3.4	6.5
101.4	8.8	3.78	6.5	3.3	3.48	6.3	3.2	3.61	4.5	3.3	5.6
126.8	12.2	3.50	5.5	3.2	3.30	5.2	3.2	3.38	3.8	3.2	5.0
163.2	17.5	3.00	4.7	3.2	2.89	4.6	3.2	2.94	3.3	3.2	4.6
217.9	26.6	2.78	7.8	6.9	2.45	8.3	6.6	2.61	5.7	6.3	8.9

Table XIV Averaged Values for the Cross-Section Ratio

$\sigma_\gamma(^{243}Am)/\sigma_\gamma(^{197}Au)$

Run	Bismuth-Graphite Converter	Graphite Converter	Average	Energy Range (keV)
I	3.50	3.52	3.51	20 - 80
II	3.47	3.52	3.49	20 - 80
III	3.58	3.54	3.57	20 - 80
IV	3.65	3.65	3.65	20 - 80
V	3.60	3.54	3.57	20 - 80
VI	3.61	3.59	3.60	20 - 80
I - VI	3.57	3.56	3.57	
VII	3.85	3.55	3.68	50 - 200
VIII	3.84	3.66	3.73	50 - 200
VII-VIII	3.85	3.61	3.71	

Table XV Absolute Values for the Capture Cross Section of ^{243}Am in the Energy Range 5 - 100 keV (Flight Path 53 mm)

Run I			Run II			Run III			Run IV		
En (keV)	$\sigma_\gamma(^{197}Au)$ (mb)	$\sigma_\gamma(^{243}Am)$ (mb)	En (keV)	$\sigma_\gamma(^{197}Au)$ (mb)	$\sigma_\gamma(^{243}Am)$ (mb)	En (keV)	$\sigma_\gamma(^{197}Au)$ (mb)	$\sigma_\gamma(^{243}Am)$ (mb)	En (keV)	$\sigma_\gamma(^{197}Au)$ (mb)	$\sigma_\gamma(^{243}Am)$ (mb)
5.7	1856.0	4072	5.7	1854.0	3080	5.6	1759.0	3178	5.8	1850.0	2679
7.5	1521.0	3343	7.5	1510.0	2576	7.3	1555.0	2869	7.6	1497.0	2719
10.1	1145.0	2906	10.2	1143.0	2699	9.9	1155.0	2841	10.3	1141.0	2928
12.9	983.5	2639	13.1	963.5	2411	12.7	999.4	2596	13.1	962.4	2827
15.7	837.9	2417	15.9	836.4	2534	15.5	841.6	2369	15.9	838.1	2448
18.3	779.4	2414	18.6	748.6	2210	18.0	813.0	2366	18.5	758.3	2409
20.6	660.0	2048	20.9	668.5	2207	20.2	664.5	2180	20.7	663.6	2181
23.2	614.6	2071	23.5	602.5	1976	22.9	613.9	2082	23.4	608.8	2119
26.4	607.1	2034	26.8	618.7	2078	26.0	608.9	2045	26.5	610.6	2189
30.2	581.5	1948	30.7	568.8	1920	29.9	587.6	1989	30.4	578.6	1978
35.0	512.5	1806	35.6	516.0	1800	34.7	514.7	1867	35.2	513.4	1912
41.1	493.1	1754	41.8	482.9	1727	40.8	496.9	1845	41.3	490.1	1849
48.8	443.9	1680	49.7	440.3	1604	48.6	439.7	1635	49.0	442.8	1662
59.0	403.2	1531	60.0	399.1	1485	58.8	407.0	1563	59.3	402.7	1592
72.8	366.6	1378	74.0	364.3	1333	72.6	367.5	1399	73.0	365.7	1398
92.1	313.2	1086	93.5	311.7	1048	91.9	313.2	1110	92.3	313.0	1038

Table XV cont.

Average				
En (keV)	σ_γ (^{243}Am) (mb)	Uncertainty (%) statistical	systematic	total
5.7	3381	9.2	16.0	18.5
7.5	2918	5.5	10.8	12.1
10.1	2836	2.8	7.5	8.0
13.0	2588	2.6	5.6	6.2
15.8	2444	1.7	4.7	5.0
18.4	2328	1.8	4.3	4.7
20.6	2160	1.4	4.2	4.4
23.3	2050	1.1	4.0	4.2
26.4	2085	0.9	3.5	3.6
30.3	1956	0.7	3.5	3.6
35.1	1842	0.6	3.4	3.5
41.3	1794	0.5	3.4	3.4
49.0	1640	0.5	3.4	3.4
59.3	1543	0.5	3.3	3.3
73.1	1377	0.5	4.3	4.3
92.5	1075	1.0	9.4	9.5

Table XVI Absolute Values for the Capture Cross Section of ^{243}Am in the Energy Range 5 - 100 keV (Flight Path 71 mm)

Run V			Run VI			Average				
								Uncertainty (%)		
En (keV)	$\sigma_\gamma(^{197}Au)$ (mb)	$\sigma_\gamma(^{243}Am)$ (mb)	En (keV)	$\sigma_\gamma(^{197}Au)$ (mb)	$\sigma_\gamma(^{243}Am)$ (mb)	En (keV)	$\sigma_\gamma(^{243}Am)$ (mb)	statistical	systematic	total
7.0	1620	4133	7.2	1578	3530	7.1	3664	8.9	11.7	14.7
8.7	1241	3044	9.0	1218	3190	8.9	3157	6.3	9.0	11.0
11.1	1104	2635	11.4	1092	2717	11.3	2699	4.2	8.6	9.6
13.5	926.4	2808	13.9	905.2	2511	13.7	2579	4.1	4.9	6.4
15.7	836.9	2373	16.1	828.2	2332	15.9	2342	3.2	4.4	5.4
17.6	814.4	2429	18.0	807.1	2382	17.8	2394	3.5	3.9	5.2
19.1	703.4	2288	19.5	676.8	2164	19.3	2191	2.9	3.7	4.7
20.8	679.9	2318	21.3	657.9	2170	21.1	2201	2.5	3.7	4.5
22.8	605.5	1968	23.3	611.7	2077	23.1	2049	2.0	3.5	4.0
25.0	610.3	2023	25.6	599.2	1967	25.3	1979	1.7	3.4	3.8
27.7	624.8	2081	28.3	624.0	2119	28.0	2109	1.4	3.1	3.4
30.7	564.0	1956	31.3	554.9	1959	31.0	1958	1.2	3.1	3.3
34.2	517.2	1883	34.9	508.8	1789	34.6	1810	1.1	3.1	3.3
38.4	521.8	1835	39.3	522.5	1900	38.9	1882	1.0	3.0	3.2
43.5	455.8	1681	44.4	448.9	1656	44.0	1663	0.9	3.0	3.1
49.5	438.8	1636	50.6	439.6	1656	50.1	1650	0.9	3.0	3.1
56.9	419.5	1605	58.3	406.6	1558	57.6	1568	0.8	3.0	3.1
66.2	380.8	1437	67.8	380.8	1465	67.0	1457	0.8	3.0	3.1
77.9	350.0	1338	79.8	340.8	1308	78.9	1315	0.9	3.8	3.9
93.1	308.9	1070	95.4	309.3	1130	94.3	1112	1.6	8.6	8.7

Table XVII — Absolute Values for the Capture Cross Section of ^{243}Am in the Energy Range 40 - 250 keV. (The Respective Uncertainties are given in Tables XII and XIII.)

Run VII			Run VIII		
En (keV)	σ_γ (^{197}Au) (mb)	σ_γ (^{243}Am) (mb)	En (keV)	σ_γ (^{197}Au) (mb)	σ_γ (^{243}Am) (mb)
34.4	515	2208	38.2	520	1805
40.3	505	1733	43.7	455	1710
47.9	437	1761	50.3	442	1650
57.8	414	1752	58.7	406	1553
71.1	371	1477	69.2	378	1528
89.7	315	1245	83.0	327	1377
116.6	291	982	101.4	308	1113
157.9	254	794	126.8	278	941
226.1	239	618	163.2	250	735
			217.9	242	630

Table XVIII Experimental Results for the Fission Cross Section of ^{243}Am Relative to ^{235}U

Energy (keV)	$\frac{\sigma_f(^{243}Am)}{\sigma_f(^{235}U)}$ ($\times 10^{-3}$)	$\sigma_f(^{235}U)$ (b)	$\sigma_f(^{243}Am)$ (mb)	Uncertainty (%)		
				Statistical	Systematic	Total
A) Averaged Data from Runs I, II, III and IV						
10 - 15	4.57	2.709	12.4	4.1	7.7	8.7
15 - 20	5.42	2.433	13.2	2.8	7.5	8.0
20 - 30	5.18	2.170	11.2	1.5	7.5	7.7
30 - 40	5.28	1.987	10.5	1.4	7.7	7.8
40 - 60	5.46	1.842	10.1	0.9	8.2	8.3
60 - 100	5.26	1.642	8.6	1.2	10.0	10.1
B) Averaged Data from Runs V and VI						
10 - 15	4.66	2.712	12.6	6.9	10.4	12.5
15 - 20	4.77	2.431	11.6	5.7	8.9	10.6
20 - 30	5.29	2.166	11.5	2.3	9.1	9.4
30 - 40	5.19	1.984	10.3	2.1	9.7	9.9
40 - 60	5.28	1.844	9.7	1.6	8.9	9.0
60 - 100	5.21	1.655	8.6	1.5	9.5	9.6
C) Data from Run VII						
30 - 40	5.82	1.995	11.6	26.0	15.9	30.5
40 - 60	7.50	1.848	13.9	10.0	15.6	18.5
60 - 100	6.19	1.645	10.2	7.0	9.8	12.0
100 - 150	8.77	1.476	12.9	3.4	9.8	10.4
150 - 250	6.71	1.356	9.1	5.5	11.1	12.4
D) Data from Run VIII						
30 - 40	5.64	1.995	11.3	32.0	12.6	34.4
40 - 60	5.48	1.847	10.1	20.0	10.3	22.5
60 - 100	7.06	1.650	11.7	8.4	8.2	11.7
100 - 150	6.50	1.476	9.6	6.8	8.8	11.1
150 - 200	5.72	1.380	7.9	9.5	9.1	13.2
200 - 250	5.62	1.322	7.4	19.7	11.4	22.8

FIGURE CAPTIONS

Fig. 1 Schematic view of the experimental setup for the capture and fission cross section measurement on ^{243}Am.

Fig. 2 Experimental TOF spectra of the ^{243}Am sample taken with two Moxon-Rae detectors with graphite and bismuth graphite converters, which were shielded by lead absorbers of various thickness. The background given in each figure is the TOF spectrum measured with the graphite sample. To these spectra a constant value has been added to account for the time independent background from the ^{243}Am decay.

These data were measured in the low energy range (5 - 100 keV) at a flight path of 53 mm.

Fig. 3a TOF spectra of the measurements in the low energy range (5 - 100 keV) at a flight path of 71 mm in the same representation as Fig. 2

Fig. 3b TOF spectra of the measurements in the high energy range (40 - 250 keV) in the same representation as Fig. 2.

Fig. 4 Experimental TOF spectra of the ^{243}Am sample taken with the fission neutron detector in the low and high energy range.

Fig. 5 The neutron capture cross section of ^{243}Am. The values given are obtained by multiplying the experimental ratios with the evaluated capture cross section of gold from ENDF/B-V. The results obtained with two Moxon-Rae detectors and different lead shieldings at a given

flight path have been combined in one data set. A comparison is made to theoretical calculations.

Fig. 6 The subthreshold fission cross section of ^{243}Am. The values given are obtained by multiplying the experimental ratios with the ^{235}U fission cross section recommended in Ref. 25.

Fig. 7 X-ray absorption spectrum of the ^{243}Am sample in the region of the K-absorption edge of plutonium. The upper limit for a possible plutonium contamination is 0.06 % on a 1σ confidence level.

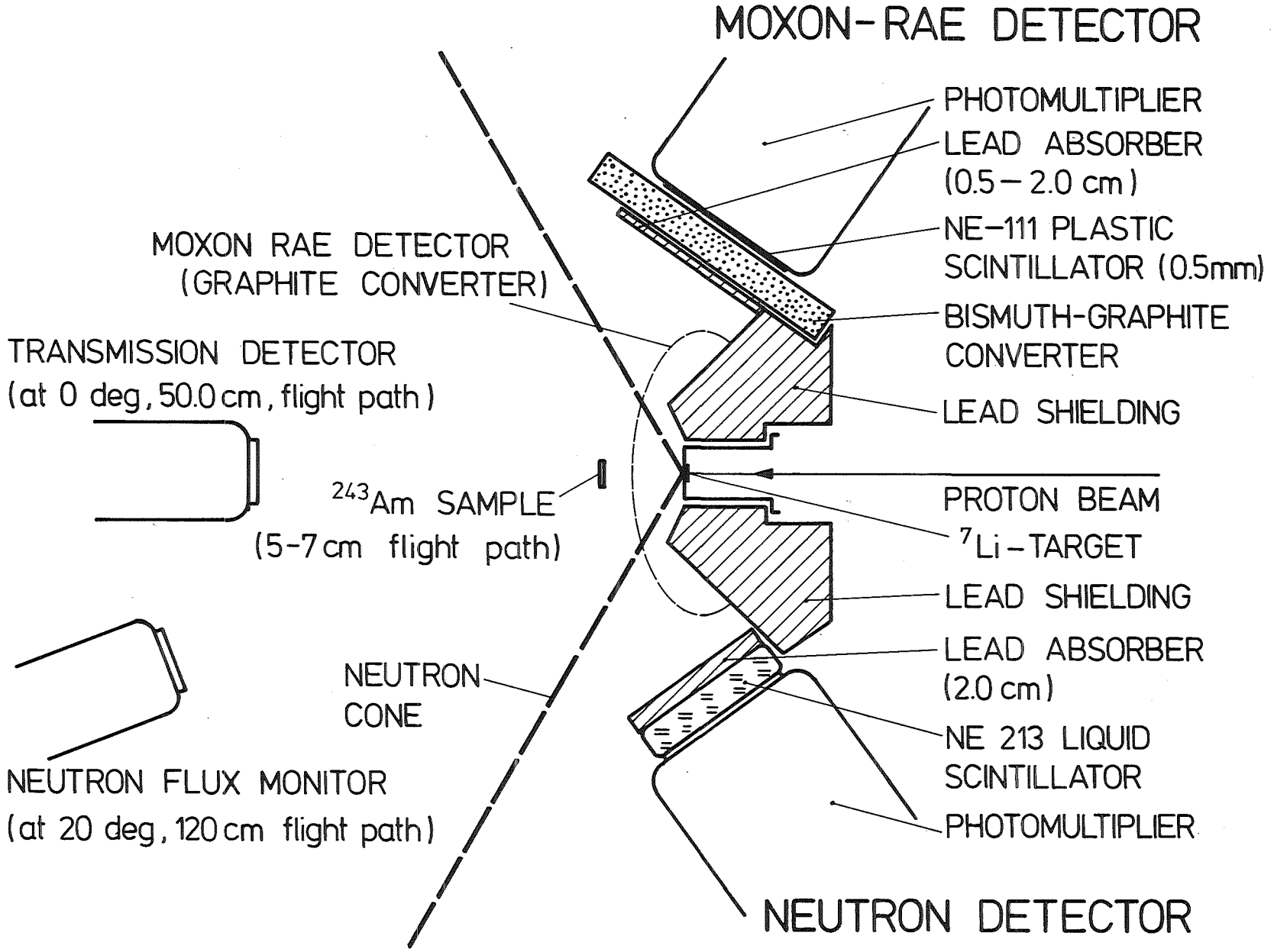
MOXON-RAE DETECTOR
PHOTOMULTIPLIER
LEAD ABSORBER
(0.5 – 2.0 cm)
NE-111 PLASTIC
SCINTILLATOR (0.5mm)
BISMUTH-GRAPHITE
CONVERTER
LEAD SHIELDING
MOXON RAE DETECTOR
(GRAPHITE CONVERTER)
TRANSMISSION DETECTOR
(at 0 deg, 50.0 cm, flight path)
^{243}Am SAMPLE
(5-7 cm flight path)
PROTON BEAM
^{7}Li – TARGET
LEAD SHIELDING
LEAD ABSORBER
(2.0 cm)
NEUTRON
CONE
NE 213 LIQUID
SCINTILLATOR
PHOTOMULTIPLIER
NEUTRON FLUX MONITOR
(at 20 deg, 120 cm flight path)
NEUTRON DETECTOR

Fig. 1

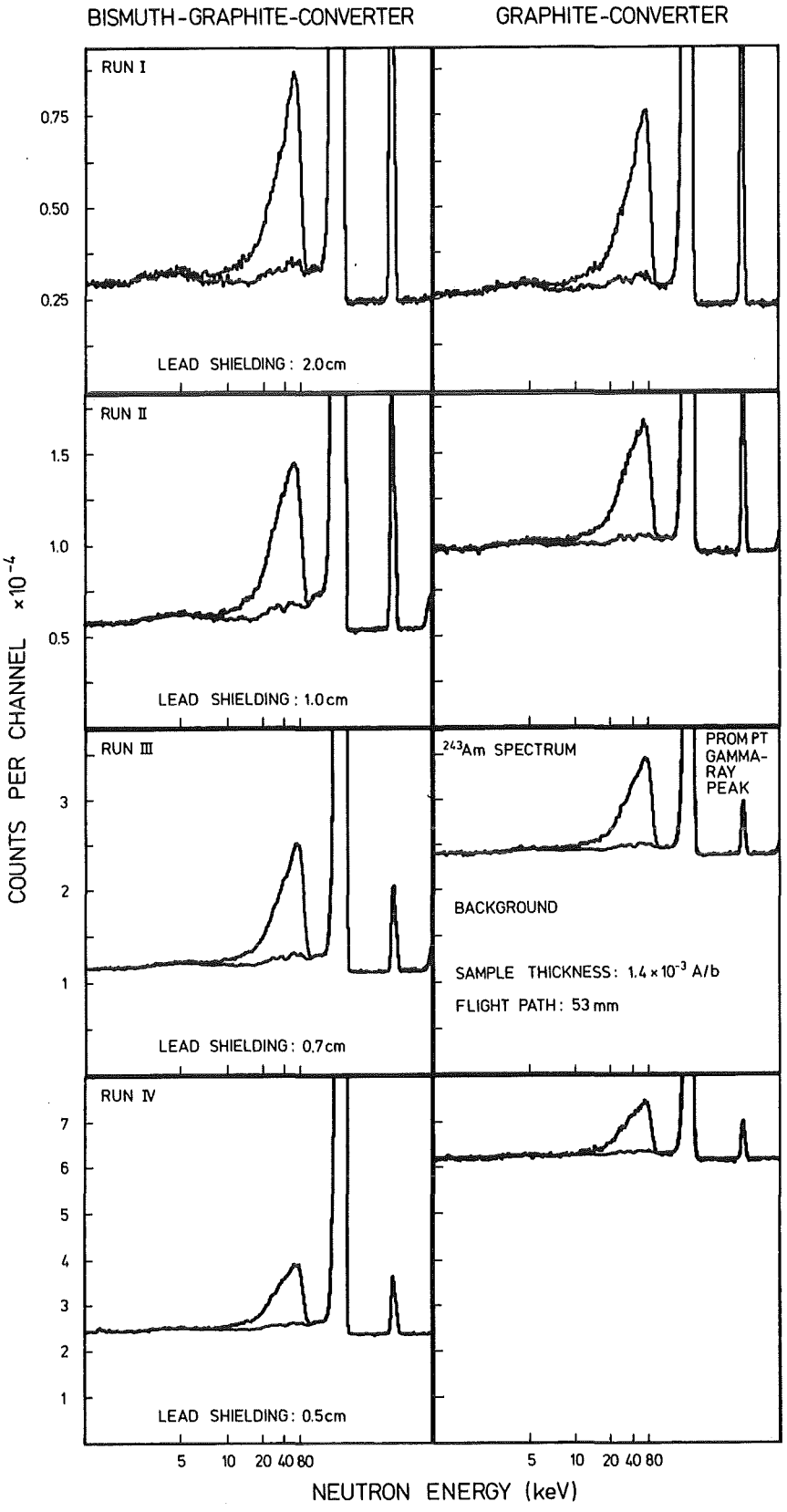
BISMUTH-GRAPHITE-CONVERTER
GRAPHITE-CONVERTER
RUN I
LEAD SHIELDING: 2.0cm
RUN II
LEAD SHIELDING: 1.0cm
RUN III
LEAD SHIELDING: 0.7cm
RUN IV
LEAD SHIELDING: 0.5cm
^{243}Am SPECTRUM
PROMPT GAMMA-RAY PEAK
BACKGROUND
SAMPLE THICKNESS: 1.4×10^{-3} A/b
FLIGHT PATH: 53 mm
COUNTS PER CHANNEL $\times 10^{-4}$
0.75
0.50
0.25
1.5
1.0
0.5
3
2
1
7
6
5
4
3
2
1
5 10 20 40 80
5 10 20 40 80
NEUTRON ENERGY (keV)

Fig. 2

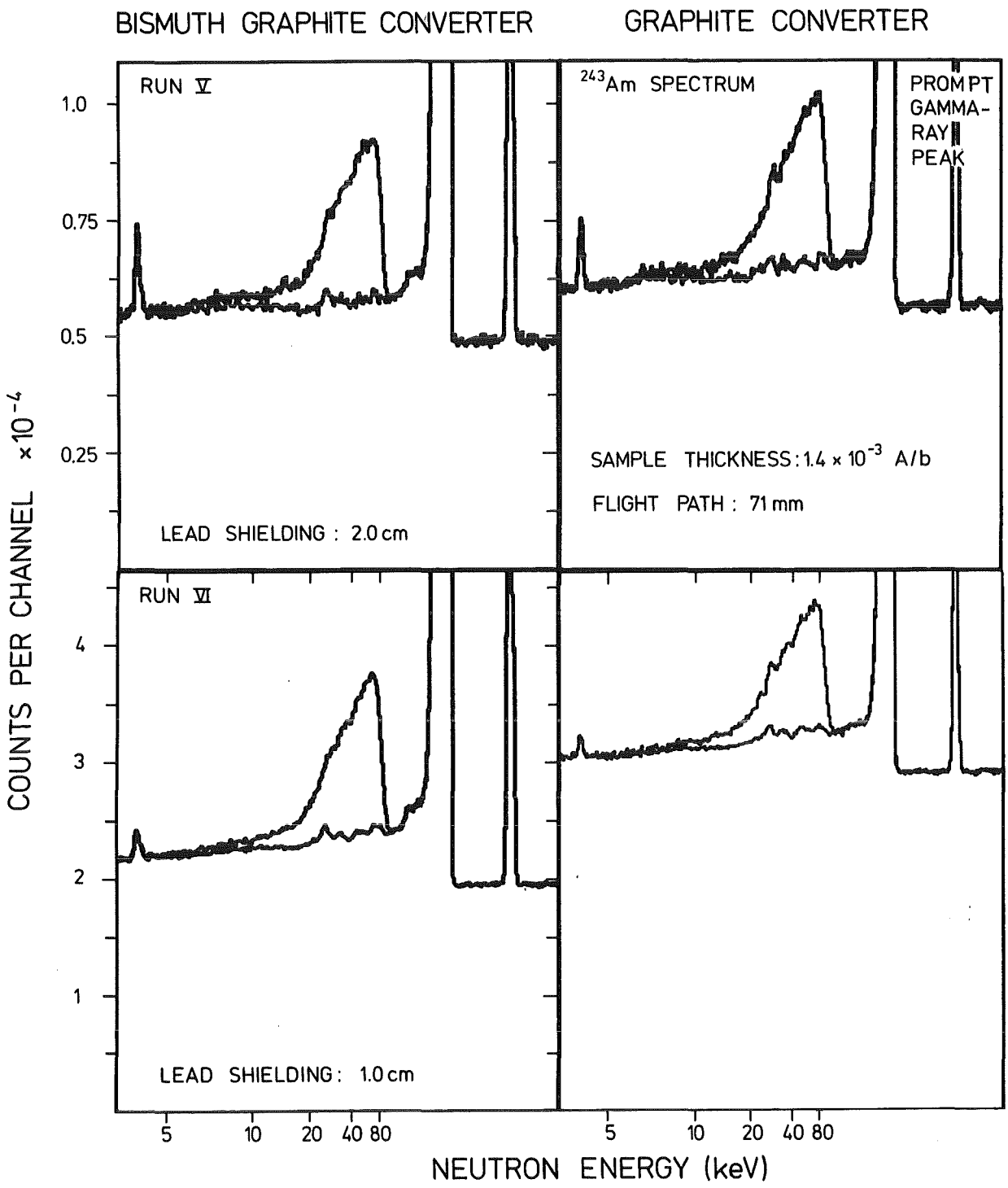
BISMUTH GRAPHITE CONVERTER
GRAPHITE CONVERTER
RUN V
^{243}Am SPECTRUM
PROMPT GAMMA-RAY PEAK
SAMPLE THICKNESS: 1.4 × 10^{-3} A/b
FLIGHT PATH : 71 mm
LEAD SHIELDING : 2.0 cm
RUN VI
LEAD SHIELDING: 1.0 cm
COUNTS PER CHANNEL ×10^{-4}
1.0
0.75
0.5
0.25
4
3
2
1
5
10
20
40
80
NEUTRON ENERGY (keV)

Fig. 3a

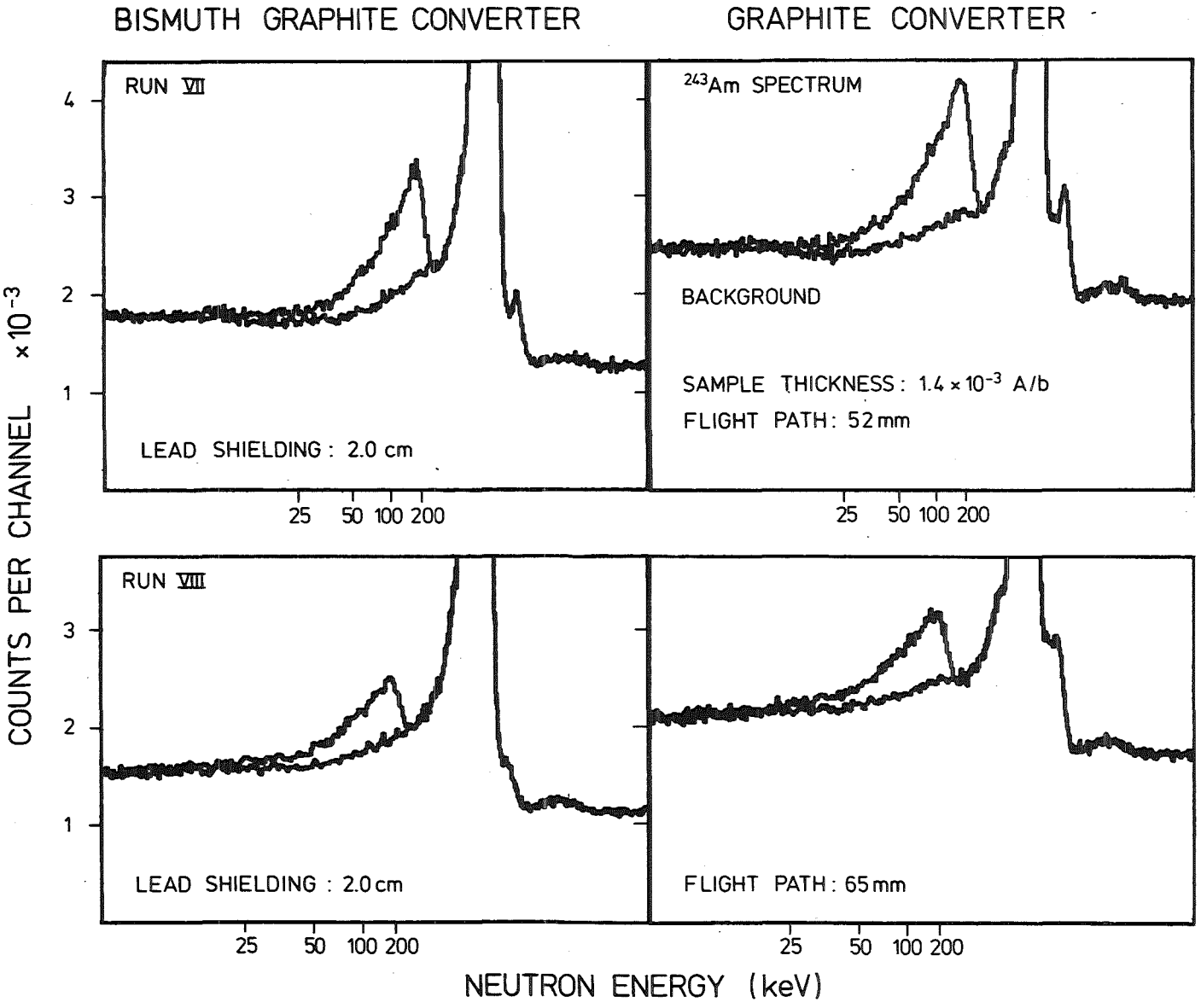
BISMUTH GRAPHITE CONVERTER
GRAPHITE CONVERTER
RUN VII
^{243}Am SPECTRUM
BACKGROUND
SAMPLE THICKNESS : 1.4 × 10^{-3} A/b
FLIGHT PATH : 52 mm
LEAD SHIELDING : 2.0 cm
RUN VIII
LEAD SHIELDING : 2.0 cm
FLIGHT PATH : 65 mm
COUNTS PER CHANNEL × 10^{-3}
NEUTRON ENERGY (keV)
25 50 100 200
1 2 3 4

Fig. 3b

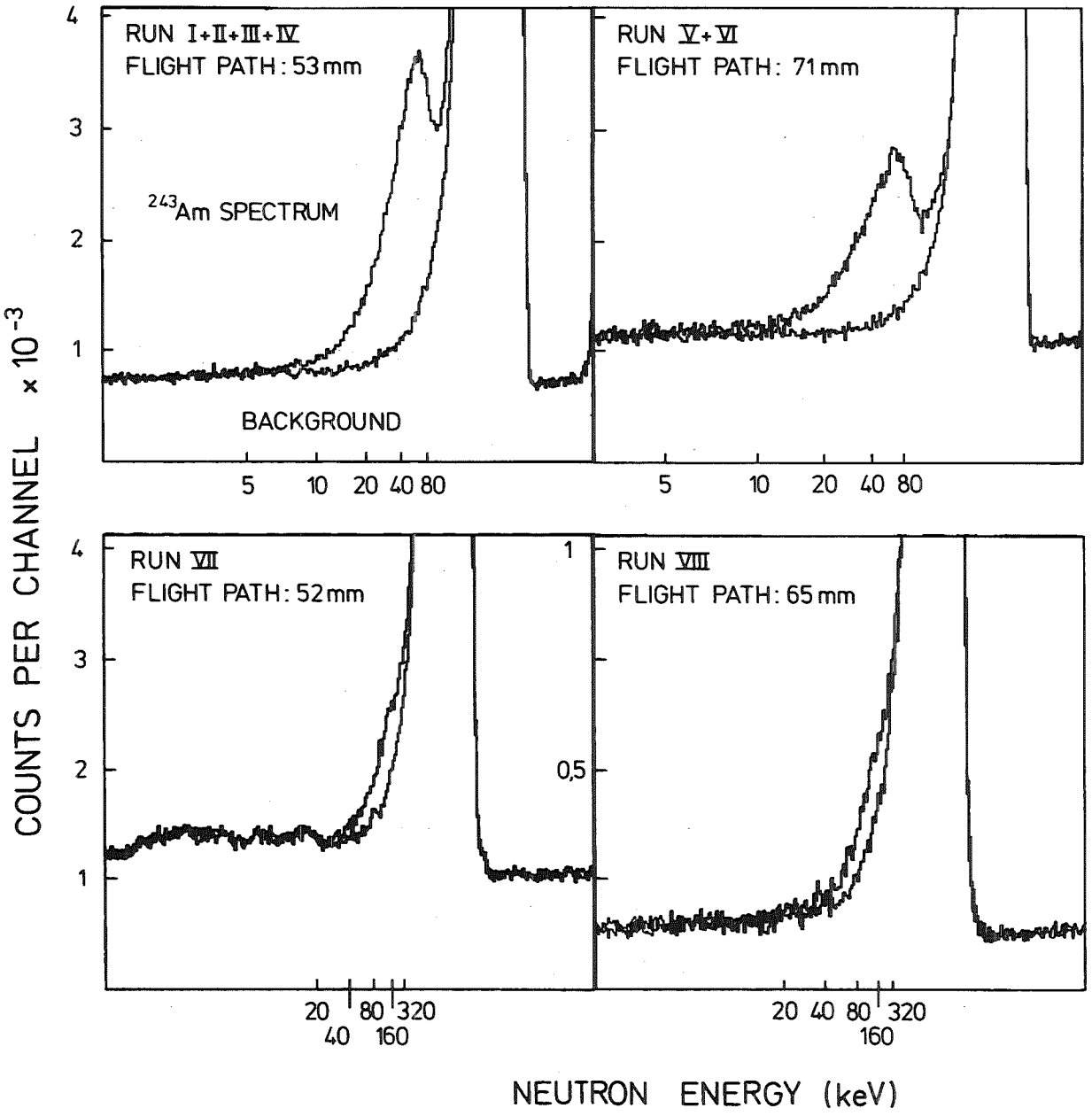
RUN I+II+III+IV
FLIGHT PATH: 53 mm
^{243}Am SPECTRUM
BACKGROUND
RUN V+VI
FLIGHT PATH: 71 mm
RUN VII
FLIGHT PATH: 52 mm
RUN VIII
FLIGHT PATH: 65 mm
COUNTS PER CHANNEL x 10^{-3}
NEUTRON ENERGY (keV)
1
2
3
4
0,5
5
10
20
40
80
160
320

Fig. 4

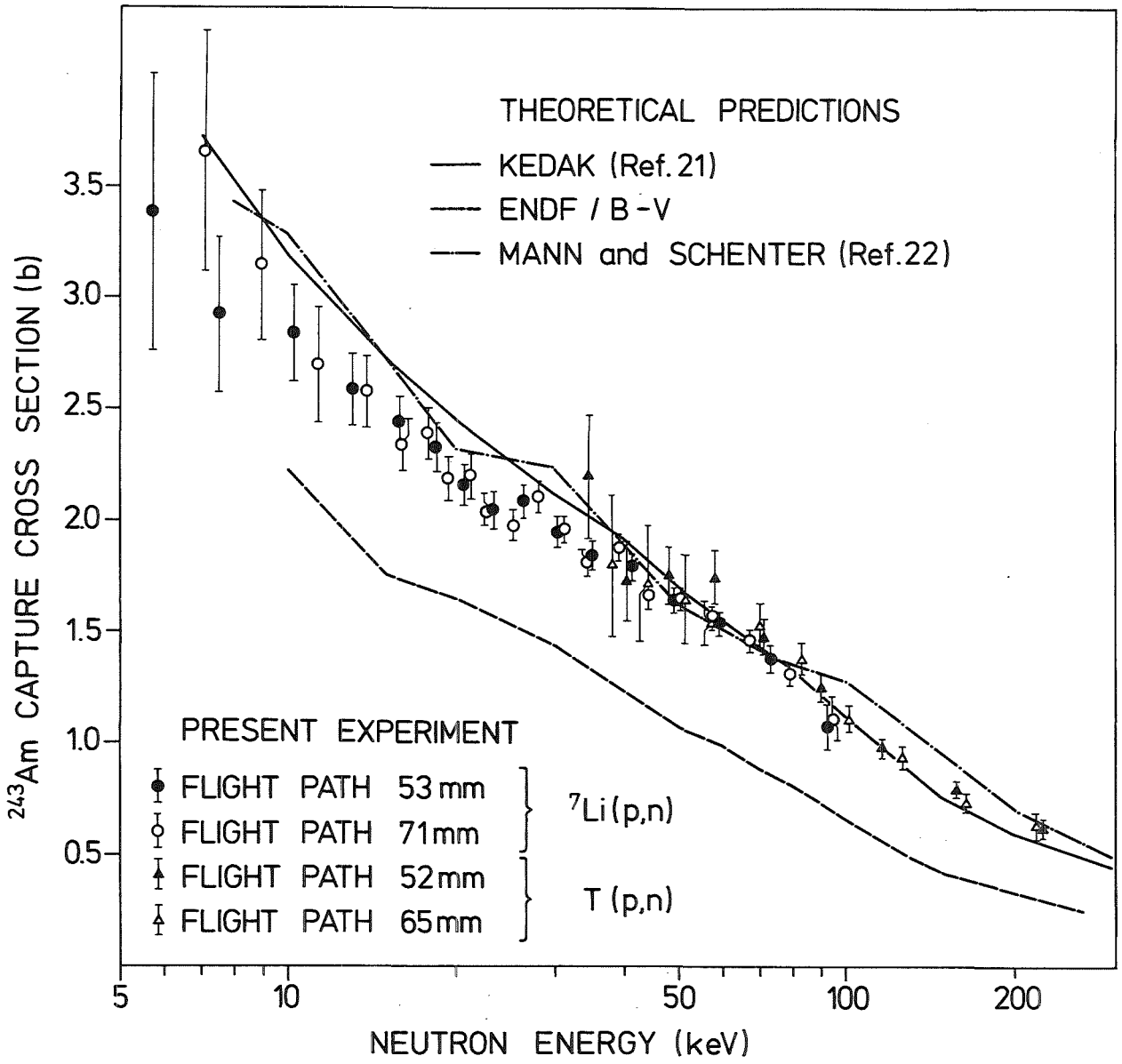
THEORETICAL PREDICTIONS
KEDAK (Ref. 21)
ENDF / B-V
MANN and SCHENTER (Ref. 22)
PRESENT EXPERIMENT
FLIGHT PATH 53 mm
FLIGHT PATH 71 mm
FLIGHT PATH 52 mm
FLIGHT PATH 65 mm
7Li(p,n)
T(p,n)
243Am CAPTURE CROSS SECTION (b)
NEUTRON ENERGY (keV)
3.5
3.0
2.5
2.0
1.5
1.0
0.5
5
10
50
100
200

Fig. 5

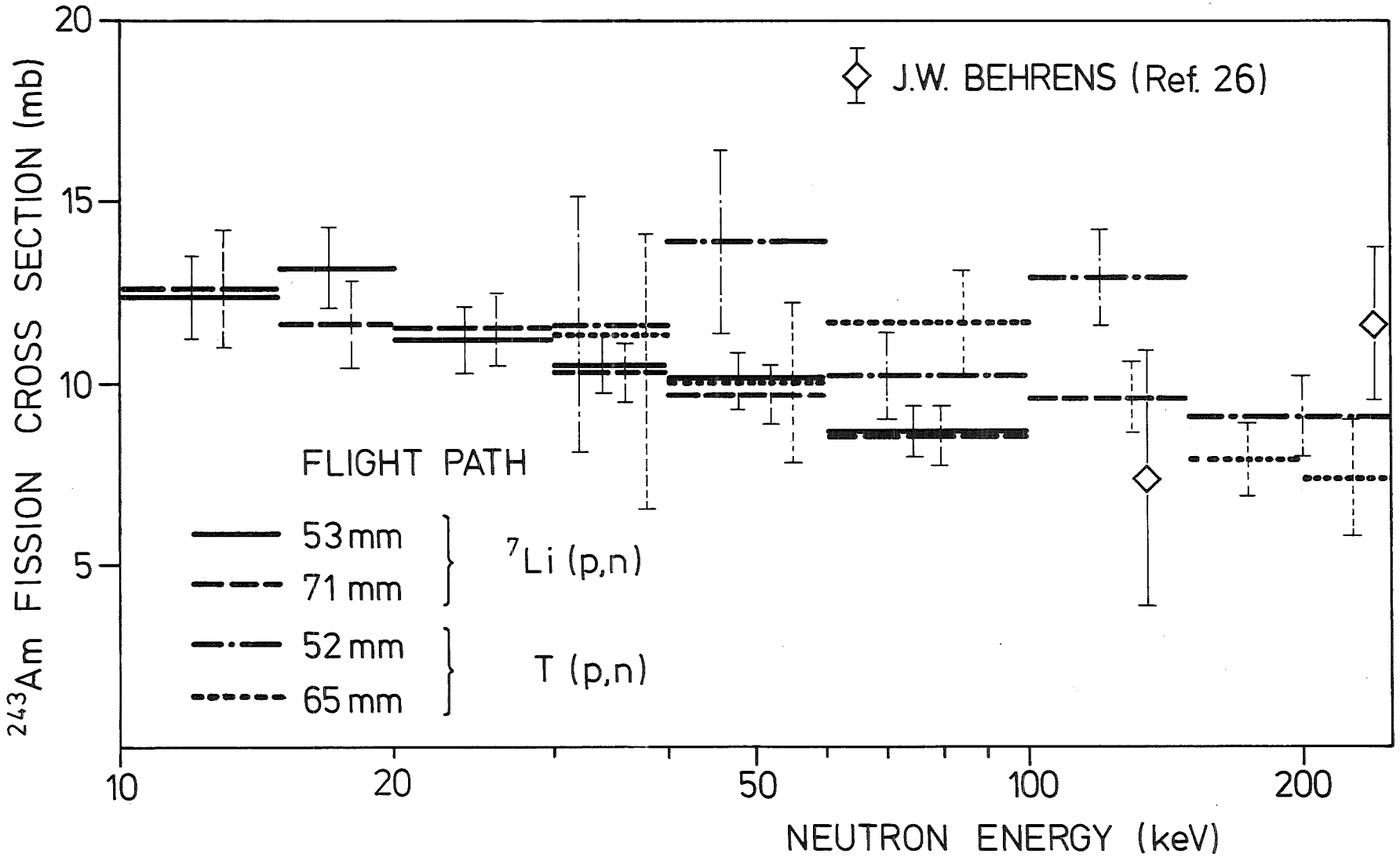
20
15
10
5
^{243}Am FISSION CROSS SECTION (mb)
J.W. BEHRENS (Ref. 26)
FLIGHT PATH
53 mm
71 mm
^{7}Li (p,n)
52 mm
65 mm
T (p,n)
10
20
50
100
200
NEUTRON ENERGY (keV)

Fig. 6

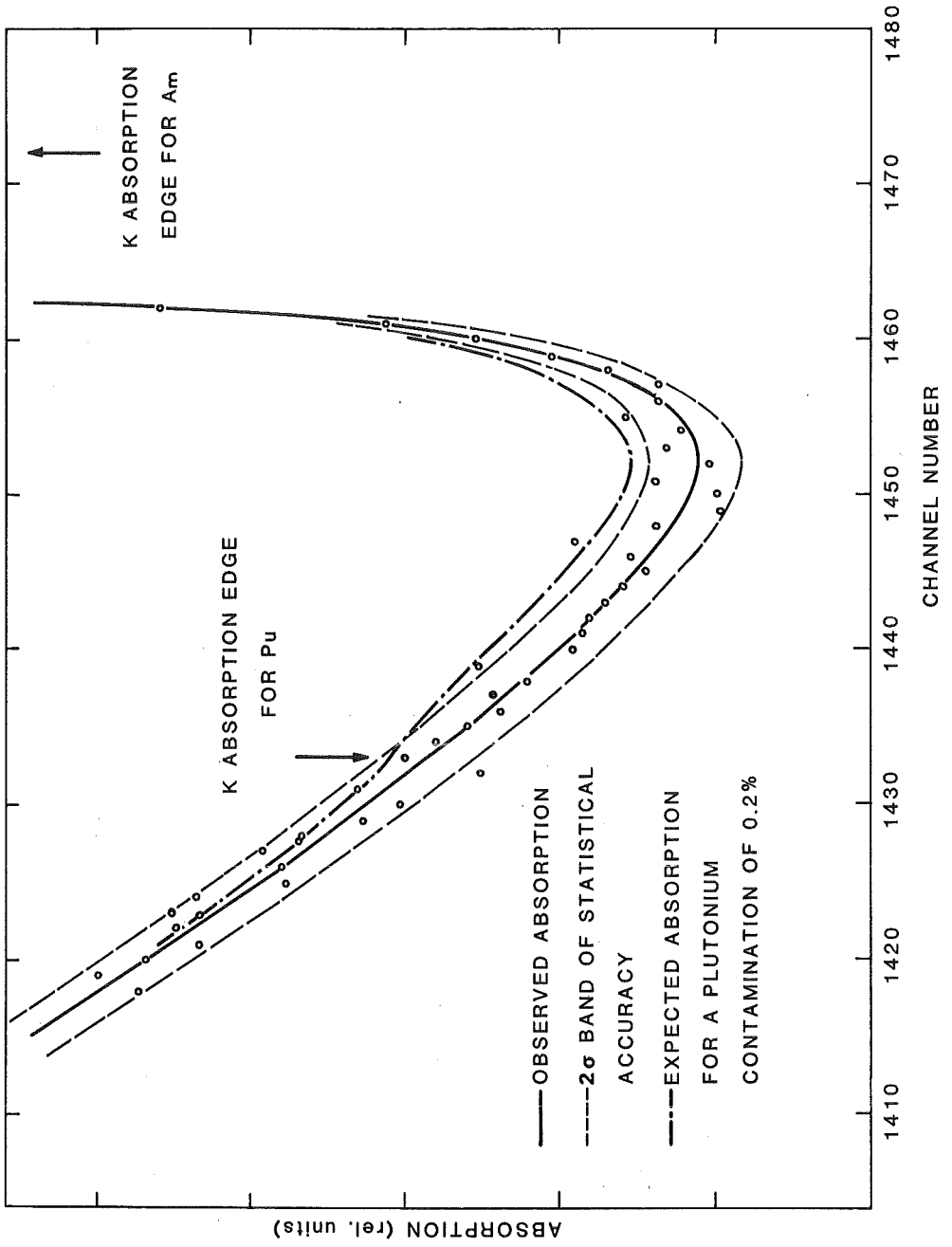
K ABSORPTION EDGE FOR Am
K ABSORPTION EDGE FOR Pu
OBSERVED ABSORPTION
2σ BAND OF STATISTICAL ACCURACY
EXPECTED ABSORPTION FOR A PLUTONIUM CONTAMINATION OF 0.2%
ABSORPTION (rel. units)
CHANNEL NUMBER
1410
1420
1430
1440
1450
1460
1470
1480

Fig. 7